THE ASTROPHYSICAL JOURNAL, 486:886–902, 1997 September 10

ASCA OBSERVATIONS OF THE BARNARD 209 DARK CLOUD AND AN INTENSE X-RAY FLARE ON V773 TAURI

STEPHEN L. SKINNER
JILA, University of Colorado, Boulder, CO 80309-0440
MANUEL GÜDEL
Paul Scherrer Institut, Würenlingen, und Villigen, CH-5232 Villigen PSI, Switzerland
KATSUJI KOYAMA
Department of Physics, Faculty of Science, Kyoto University, Sakyo-ku, Kyoto 606-01, Japan
AND
SHIGEO YAMAUCHI
Faculty of Humanities and Social Sciences, Iwate University, 3-18-34 Ueda, Morioka, Iwate 020, Japan
Received 1997 February 11; accepted 1997 April 10

ABSTRACT

ASCA detected an intense X-ray flare on the weak-lined T Tauri star V773 Tau (=HD 283447) during a 30 ks observation of the Barnard 209 dark cloud in 1995 September. This star is a spectroscopic binary (K2 V + K5 V) and shows signs of strong magnetic surface activity including a spot-modulated optical light curve. The flare was seen only during its decay phase but is still one of the strongest ever recorded from a T Tauri star with a peak luminosity $L_X = 10^{32.4}$ ergs s^{-1} (0.5–10 keV), a maximum temperature of at least 42 million K, and energy release $\gtrsim 10^{37}$ ergs. A shorter *ASCA* observation taken five months later showed V773 Tau in a quiescent state ($L_X = 10^{31.0}$ ergs s^{-1}) and detected variable emission from the infrared binary IRAS 04113+2758.

The differential emission measure (DEM) distribution during the V773 Tau flare shows a bimodal temperature structure that is almost totally dominated by hot plasma at an average temperature of ≈ 37 million K. Using information from time-resolved spectra, we examine the flare decay in terms of solar flare models (cooling loops and two-ribbon flares) and also consider possible nonsolar behavior (interbinary flares, star-disk flares, and rotational X-ray modulation). Solar models are unable to reproduce the unusual convex-shaped X-ray light curve, which decays slowly over a timespan of at least 1 day. However, the light curve decay is accurately modeled as a sinusoid with an inferred X-ray period of 2.97 days, which is nearly identical to the optical rotation period(s) of the two K-type components. This provides tantalizing evidence that the flaring region was undergoing rotational occultation, but periodic X-ray variability is not yet proven since our *ASCA* observation spans only one-third of a rotation cycle.

Subject headings: ISM: individual (L1495) — stars: coronae — stars: individual (HD 283447, V773 Tau) — stars: pre–main-sequence — X-rays: stars

1. INTRODUCTION

The fickle personalities and diverse phenomenology of T Tauri stars are by now well-known to astronomers but still continue to provide us with new discoveries. A particularly striking example is V773 Tau (=HD 283447), lying within the Barnard 209 dark cloud. After years of study, this star was recently found by Welty (1995) to be a double-lined spectroscopic binary (K2 V + K5 V). In a contemporaneous VLBI/VLA radio study, Phillips et al. (1996) resolved the 3.6 cm radio emission into two components that may correspond to the individual K stars. Surprisingly, this VLBI/VLA study also showed that the radio emission of V773 Tau is both circularly and *linearly* polarized. Although circular polarization and radio flaring have previously been reported in V773 Tau (White, Pallavicini, & Kundu 1992), the detection of linearly polarized radio emission is so far unique among T Tauri stars.

By all indications, the magnetic surface activity on V773 Tau is extreme and the reasons for this are not yet clear. The presence of highly variable nonthermal radio emission that is both circularly and linearly polarized is an unambiguous signature of an ordered magnetic field. Magnetic surface activity is also revealed in the optical light curve, which shows a quasi-sinusoidal rotational modulation. This optical variability has been attributed to large photospheric spots (Rydgren & Vrba 1983). In the framework of solar-like activity, such spots are thought to arise in regions of high magnetic field strength where convective energy transport from below is partially blocked (Bertout 1989; see also Herbst et al. 1994).

Magnetic surface activity in late-type stars often reveals itself in the form of coronal X-ray emission, and V773 Tau is indeed known to be a strong X-ray source. It was detected in the *ROSAT* all-sky survey (Neuhäuser et al. 1995) and in a more sensitive *ROSAT* PSPC pointed observation on 1992 September 11 (Feigelson et al. 1994). Spectral fits of the PSPC data using optically thin plasma models showed evidence for a multitemperature plasma with the hottest component at a temperature of 16 (14–35) million K (parentheses hereafter enclose 90% confidence limits). The *ROSAT* PSPC data showed no significant X-ray variability during the 6.7 hr spanning the observation, whereas simultaneous VLA monitoring revealed a slow monotonic decline in the 3.6 cm radio luminosity by a factor of 4. This

apparent decoupling between the radio and X-ray variability contrasts sharply with the correlated variability seen in other magnetically active systems such as dMe flare stars (Güdel et al. 1996) and RS CVn binaries (Brown et al. 1996).

Ultimately, one would like to know whether the full range of magnetic behavior in V773 Tau can be described in terms of scaled-up solar-like activity, or whether more exotic processes such as star-disk or star-star magnetospheric coupling must be invoked. To address this question, additional observations are needed since the recent discoveries cited above indicate that the full range of magnetically induced activity in this remarkable system has not yet been sampled. In particular, we note that X-ray sampling in the time domain is particularly sparse since the previous *ROSAT* observations have covered less than 10% of the ≈ 2.9 day K-star rotation cycles (§ 2).

We report here the results of two recent X-ray observations of the Barnard 209 dark cloud acquired with *ASCA* in 1995 September (30 ks) and 1996 February (10 ks), spanning approximately 23 and 8 hr, respectively. In both observations the pointing was centered on V773 Tau. Our objectives were (1) to search for evidence of X-ray variability with emphasis on identifying any slow component that might have been missed in the shorter *ROSAT* exposures, and (2) to accurately determine the temperature and emission measure distribution in the X-ray emitting plasma, with particular emphasis on the hot component that was detected by *ROSAT*.

These new *ASCA* observations show that the X-ray emission of V773 Tau is highly variable and can change by a factor of ~ 3 over one day and by more than an order of magnitude over five months. Using time-resolved spectra, we analyze the slow decay of an intense X-ray flare that was detected in our initial observation and trace this decay to a steady drop in the emission measure of a superhot plasma component whose maximum temperature exceeded ~ 40 MK. We discuss the flare decay in terms of conventional models based on the solar analogy (quasi-static cooling loops and two-ribbon flares), and also consider the relevance of unconventional models (interbinary flares, star-disk magnetic reconnection, and rotational modulation).

2. STELLAR PROPERTIES

Table 1 summarizes the stellar properties of V773 Tau, which lies in the Barnard 209 dark cloud (= Lynds 1495 W, Lynds 1962; Duvert et al. 1986). Recent radio astrometry measurements give a precise distance of 148.5 ± 5 pc (Lestrade et al. 1997), and we will adopt a distance of 150 pc to allow a direct comparison with earlier work. V773 Tau is usually classified as a weak-lined T Tauri star (WTTS) on the basis of its weak Hα emission (Herbig & Bell 1988).

The optical light curve shows a quasi-sinusoidal modulation at a period of 3.43 days (Rydgren & Vrba 1983), which was attributed to the presence of cool starspots covering $\approx 17\%$ of the stellar surface. Welty (1995) discovered that V773 Tau is a spectroscopic binary (SB2: K2 V + K5 V), with an orbital period of 51.075 days and a semimajor axis $a = 0.343$ AU. The orbit is eccentric ($e = 0.267$) and is viewed at moderately high inclination ($\geq 65°$). Welty's upper limits for the stellar rotation periods of 2.96 days (K2) and 2.89 days (K5) are somewhat lower than the original value of 3.43 days quoted above, but these upper limits are nearly identical to the X-ray period derived here.

V773 Tau has a weak near-infrared excess (Strom et al. 1989) and may also be an *IRAS* source (Prusti et al. 1992), but the *IRAS* identification is somewhat uncertain. Near-infrared excesses in T Tauri stars are commonly attributed to circumstellar disks, but this interpretation must be treated cautiously for V773 Tau. Several factors conspire to make the interpretation of the near-IR excess complex, including (1) spectroscopic binarity, (2) the close proximity of a third near-IR source (see below), (3) cool photospheric spots (see Wolk & Walter 1996 for implications), and (4) the unusual nonthermal nature of the millimeter emission (Dutrey et al. 1996; see also § 5.2.2).

A third nearby infrared source is visible in K band at an offset of 0.″11–0.″17 (Leinert et al. 1993; Ghez, Neugebauer, & Matthews 1993). In addition, the classical T Tauri star FM Tau lies at an offset of $\approx 38''$. These sources cannot be spatially resolved by *ASCA*, but a higher resolution *ROSAT* PSPC observation shows that less than 5% of the V773 Tau count rate during quiescence is due to FM Tau

TABLE 1

OPTICAL AND INFRARED PROPERTIES OF V773 TAURI

Property	Value	Reference
Names	V773 Tau, HD 283447, HBC 367	1
Optical position (1950.0)	$04^h11^m07^s.29$, $+28°04'41''.2$	1
Spectral type	SB2: K2 V + K5 V	2
IR companion	K-band companion offset 0.″11–0.″17	3, 4
V (mag)	10.62–10.87	6, 7, 8
A_V (mag)	1.37	2, 9
Distance (pc)	148.5 ± 5	5
$M \sin^3 i$ ($M_\odot$)[a]	1.17 (K2) + 0.89 (K5)	2
M ($M_\odot$)[b]	1.73 (K2) + 0.97 (K5)	2
Radius ($R_\odot$)	2.42 (K2) + 2.39 (K5)	2
$v \sin i$ (km s^{-1})	41.4 (K2) + 41.9 (K5)	2
L_* ($L_\odot$)	3.01 (K2) + 1.90 (K5)	2
P_{rot} (days)	≤ 2.96 (K2) + ≤ 2.89 (K5)	2
P_{orb} (days)	51.075	2
Semimajor axis (AU)	0.343	2
Eccentricity	0.267	2

[a] From orbit solution.

[b] From evolutionary tracks.

REFERENCES.—(1) Herbig & Bell 1988; (2) Welty 1995; (3) Leinert et al. 1993; (4) Ghez et al. 1993; (5) Lestrade et al. 1997; (6) Rydgren & Vrba 1983; (7) Hartigan et al. 1994; (8) Martín et al. 1994; (9) Cabrit et al. 1990.

(Feigelson et al. 1994). No variability in V773 Tau was detected during this *ROSAT* observation, which spanned 6.7 hr (1.7 hr on-source). The X-ray flux measured for V773 Tau by *ROSAT* was $F_X = 1.8 \times 10^{-12}$ ergs cm^{-2} s^{-1} (0.2–2.0 keV). The *ROSAT* PSPC spectrum was fitted with a two-temperature optically thin thermal plasma with a cool component at $T_1 = 4$ (2–10) million K and a hot component with an uncertain temperature $T_2 = 16$ (14–35) million K.

3. *ASCA* X-RAY OBSERVATIONS

Two separate *ASCA* observations of the Barnard 209 dark cloud were obtained using identical pointing coordinates centered on V773 Tau. All four instruments were operating in parallel, consisting of two solid-state imaging spectrometers (SIS0 and SIS1) and two gas-imaging spectrometers (GIS2 and GIS3). Table 2 summarizes the observations and gives relevant data for the SIS0 instrument, which provided the highest signal-to-noise ratio (S/N).

A description of *ASCA* and its instrumentation is given by Tanaka, Inoue, & Holt (1994). The SIS and GIS passbands are $\approx$0.5–10 keV and $\approx$0.8–11 keV. The SIS provide better energy resolution, which is $\Delta E/E \approx 3.5\%$ (FWHM) at 6.7 keV as of mid-1995, and which scales roughly as $1/E^{1/2}$ (Dotani et al. 1996). The SIS spatial resolution of $\approx 1'$ at 5.9 keV is superior to that of the GIS but is achieved at the expense of a smaller field of view ($11' \times 22'$ for each 2 CCD SIS image, and a circular region of $40'$ usable diameter for each GIS image). Our spectral analysis will focus mainly on SIS results because of the higher SIS energy and spatial resolutions, and the better SIS sensitivity at low energies below ~ 1 keV.

Data reduction followed standard procedures using the ASCASCREEN (vers. 0.37) and XSELECT (vers. 1.3) processing scripts, and FTOOLS (vers. 3.5) software. Spectra and light curves were extracted using circular regions centered on the source peak of radii 3.8 (SIS) and 5.9 (GIS), and background was taken in source-free detector regions well away from the primary source peak. Final results were not sensitive to the precise region used to extract the background. Since the earth elevation constraints are more stringent for SIS ($\geq 25°$) than for GIS ($\geq 10°$), there is less usable exposure time for SIS.

Spectra were rebinned to 512 energy channels for SIS and 256 channels for GIS data and then further regrouped to a minimum of 10 photons per energy bin for spectral fitting and χ^2 error analysis. Response matrices were corrected for time-dependent effects (task SISRMG) and for source positioning on the individual detectors using effective area curves generated by the task ASCAARF.

4. RESULTS AND ANALYSIS

4.1. *Images*

Figures 1 and 2 show the broadband (0.7–10 keV) and hard-band (3–10 keV) GIS images for both observations. The difference between the two images taken five months apart is dramatic. The exposure on 1995 September 16–17 (Fig. 1) is totally dominated by the intense hard emission from a source whose spatial distribution of photons is pointlike to within the GIS spatial resolution. The X-ray position obtained by averaging the measurements from SIS0 and SIS1 (which have lower distortion and more accurate focal plane calibration than GIS) is R.A. (1950) = $04^h11^m10^s.67$, Decl. (1950) = $+28°04'42''.1$, with a 90% error circle of radius $40''$ (Gotthelf 1996). The nearest cataloged optical/IR object is V773 Tau, which lies at an offset of $44''.7$ from the X-ray peak at position R.A. (1950) = $04^h11^m07^s.29$, Decl. (1950) = $+28°04'41''.2$ (Herbig & Bell 1988). Thus, V773 Tau is the most likely source of the X-ray emission, even though its optical position lies slightly outside of the X-ray error circle. The only other known optical/IR source in this vicinity is the classical TTS FM Tau, which lies at a larger offset of $53''$ from the X-ray peak.

The image from the shorter exposure on 1996 February 13 is more suitable for image analysis and source identification (Fig. 2). V773 Tau is still clearly present but its count rate is an order of magnitude below that of the initial observation. The X-ray position in this exposure is in slightly better agreement with the V773 Tau optical position, having an offset of $39''.7$. Further confidence that this source is indeed V773 Tau is obtained by comparing its *ASCA* SIS flux in the soft 0.3–2.5 keV band with that measured for V773 Tau from higher resolution *ROSAT* images. We obtain a soft-band flux of 1.75×10^{-12} ergs cm^{-2} s^{-1} from SIS, which is nearly identical to that of 1.8×10^{-12} ergs cm^{-2} s^{-1} measured for V773 Tau by *ROSAT* in the same bandpass (Feigelson et al. 1994).

Three other weaker sources are also detected at S/N ≥ 5, and their most probable optical/IR identifications based on

TABLE 2

SUMMARY OF *ASCA* OBSERVATIONS OF V773 TAU[a]

Parameter	First Pointing	Second Pointing
Start date/time	1995 Sep 16/1601 UT	1996 Feb 13/0406 UT
Stop date/time	1995 Sep 17/1521 UT	1996 Feb 13/1142 UT
SIS mode	2 CCD	2 CCD
Exposure time (s)	21111	9985
Counts[b]	29904	1297
Raw count rate (counts s^{-1})	1.42[c]	0.13
Corrected count rate (counts s^{-1})[d]	1.45[c]	0.17
Hardness ratio[e]	−0.37	−0.49

[a] Data are for SIS0 detector, which provides highest signal-to-noise ratio. The quoted count rates and hardness ratios are time-averaged over entire observation.

[b] Within a circular region of radius = 3.8 centered on the V773 Tau X-ray peak (source + background).

[c] Count rate is variable.

[d] Corrected for vignetting and point spread function.

[e] Hardness ratio = $(h - s)/(h + s)$, where h = counts (2.0–10.0 keV) and s = counts (0.4–2.0 keV).

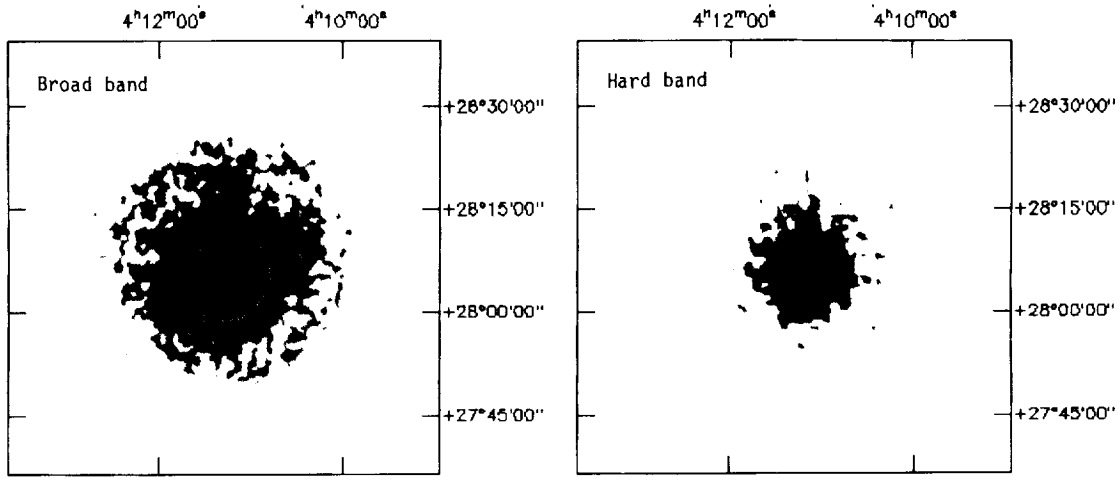

FIG. 1.—Smoothed *ASCA* images of the Barnard 209 dark cloud on 1995 September 16–17, combining photons from the GIS2 and GIS3 detectors. Left panel is broadband (0.7–10 keV), and right panel is hard-band (3–10 keV). Image is totally dominated by the bright emission from V773 Tau. The coordinate overlay (equinox 1950.0) is uncertain by $\approx 30''$ in each coordinate. Usable exposure time is ≈ 23 ks per GIS.

a search of the SIMBAD data base are given in Table 3. These are (1) the nebulous WTTS Anon 1 (=HBC 366), with spectral type M0 V, (2) the infrared source IRAS 04113+2758, a low-mass object that is known to be a binary at 2 μm (Kenyon et al. 1990), and (3) a soft X-ray source lying $\approx 5'$ east of IRAS 04113+2758 with no known optical/IR counterpart within a 2′ search radius. With the exception of this latter object, all sources show significant hard emission in the 3–10 keV band. The X-ray properties of Anon 1 and IRAS 04113+2758 are discussed further in § 4.4.

Examination of the archived *ROSAT* PSPC image taken on 1992 September 11 shows clear detections of V773 Tau, Anon 1, and IRAS 04113+2758 as well as a probable detection of the unidentified soft source. The good correspondence between the *ROSAT* image and the *ASCA* image obtained on 1996 February 13 allows a direct comparison of the source positions. We find a systematic offset in positions, with *ASCA* positions shifted westward by an amount ΔR.A. $= +2.7^{+0.3}_{-0.4}$ s relative to *ROSAT*. A similar shift is noted when comparing *ASCA* and optical positions (Table 3). Positional offsets have been noted in other *ASCA* images, and the origin of these position errors has been discussed in detail by Gotthelf (1996). If the *ASCA* positions listed in Table 3 are corrected for the 2.7 s offset in R.A., then the difference between optical and *ASCA* positions for V773 Tau is reduced to 4.″2, giving much higher confidence in the source identification.

4.2. *X-Ray Light Curves of V773 Tau*

Figure 3 shows the broadband SIS0 light curve for the flare on 1995 September 16–17. The 10.5 hr data gap beginning at $t \approx 18.5$ hr was due to last-minute cancellation of deep-space network ground station support. The pre-gap portion of the light curve ($t \leq 18.5$ hr) shows a nearly constant count rate of 2.10 counts s^{-1}, whereas the post-gap segment ($t \geq 28$ hr) shows a clear decay that continues until the end of the observation. However, closer inspection of the hard-band light curve in Figure 4 shows that the decay was already in progress at the beginning of the observation, and this is confirmed by time-partitioned flux measurements (§ 4.3.2).

A very obvious feature of the broadband light curve shown in Figure 3 is that its shape is *convex*, with almost all

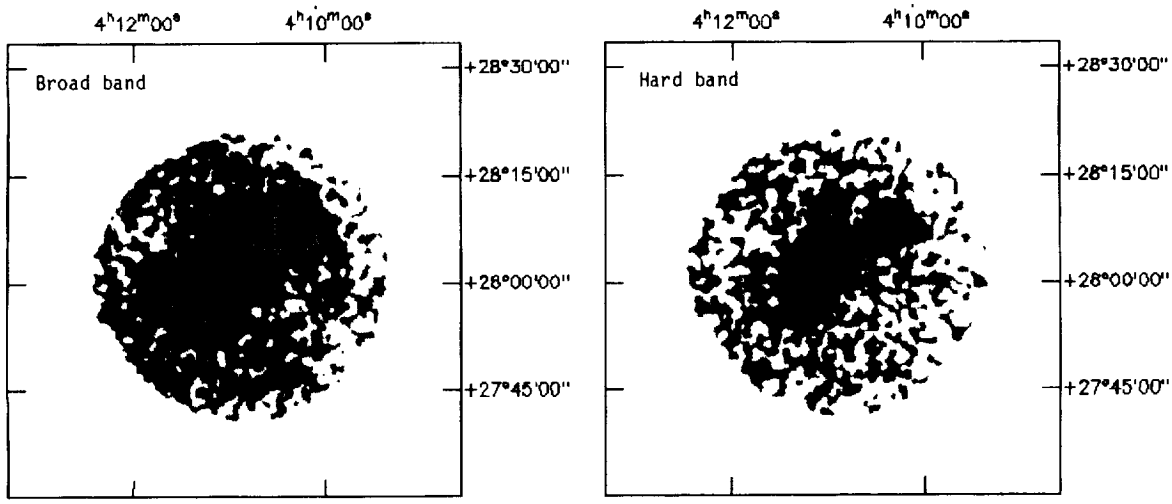

FIG. 2.—Smoothed *ASCA* images of the Barnard 209 dark cloud on 1996 February 13, combining photons from the GIS2 and GIS3 detectors. Left panel is broadband (0.7–10 keV), and right panel is hard-band (3–10 keV). Brightest source at center is V773 Tau, with 04113+2758 just below it and Anon 1 to its upper right. The coordinate overlay (equinox 1950.0) is uncertain by $\approx 30''$ in each coordinate. Usable exposure time is ≈ 12 ks per GIS.

TABLE 3

ASCA X-RAY DETECTIONS IN BARNARD 209[a]

Number	X-Ray Position (1950.0)	Optical/IR ID	Reference	Offset	Counts	Flux[b]
1.....	04 10 19.2, +28 08 44.1	Anon 1 (HBC 366)	1	+2.3, −22.6	350	2.3[c]
2.....	04 11 04.3, +28 04 39.9	V773 Tau (HBC 367)	1	+3.0, +01.3	741	2.9[d]
3.....	04 11 18.0, +27 58 58.9	IRAS 04113+2758	2	+2.9, −18.0	368	2.3
4.....	04 11 41.8, +27 58 46.9	...	...	...	108	...

[a] Values are averages of GIS2/GIS3 measurements on 1996 February 13, unless otherwise noted. X-ray positions have a 90% confidence error circle of radius ≈40″. References for optical/IR positions are: (1) Herbig & Bell 1988; (2) Kenyon et al. 1990. Position offsets are in the sense of (optical − X-ray). Counts (per GIS) are background-corrected, but not corrected for vignetting or PSF effects. Usable GIS exposure time was 12206 s.

[b] Flux units are 10^{-12} ergs cm^{-2} s^{-1} and quoted values are not corrected for absorption.

[c] SIS measurement (0.5–10 keV). Absorption-corrected flux is 2.6×10^{-12} ergs cm^{-2} s^{-1}. Anon 1 lies near edge of GIS field of view and is strongly vignetted.

[d] SIS measurement (0.5–10 keV). See Tables 2 and 4 for complete flux and count rate information.

points on the light curve lying above a line connecting the first and last data points. This immediately rules out a simple exponential decay. Indeed, we find that the full light curve can *not* be fitted using either an exponential decay ($\chi^2_{\rm red} = 1.74$ with 136 dof) or a power-law decay ($\chi^2_{\rm red} = 2.66$ with 137 dof). However, if the fit is restricted to the post-gap segment then an exponential decay model becomes marginally acceptable with an *e*-folding time of ≈12.5 hr ($\chi^2_{\rm red} = 1.24$ with 107 dof). The simplest model that is capable of fitting the entire light curve is a constant term + sinusoid (Fig. 3), with a best-fit functional form of $A(t) = 1.13 (\pm 0.07) + 0.98(\pm 0.06)$ sin $[2\pi(t - 1.15)/71.2]$ counts s^{-1} ($\chi^2_{\rm red} = 1.17$ with 136 dof), where t is in units of hr. The derived period is $71.2^{+\cdots}_{-18.9}$ hr ($= 2.97^{+\cdots}_{-0.79}$ days), where the lower limit is 90% confidence and the ellipsis signifies that no useful upper limit was obtained because of limited rotational phase coverage. The derived X-ray period is nearly identical to the *upper limits* on the optical period of 2.96 and 2.89 days obtained for the K2 and K5 components by Welty (1995). These upper limits must be multiplied by the unknown stellar inclination term sin*i* to obtain the actual optical period and the optical and X-ray periods are in good agreement if the active star is being viewed nearly equator-on ($i \approx 90°$).

Figure 4 shows the hard and soft-band light curves for the September 16–17 flare as well as the ratio of hard/soft counts (H/S). There is a discernible difference between the shapes of the soft and hard-band light curves, with the hard-band light curve showing a more erratic decay. The ratio H/S was slightly higher at the beginning of the observation when the count rate was at its maximum. This is consistent with our analysis of the time-partitioned spectra (§ 4.3), which gives maximum flare temperatures at the beginning of the observation. There is also some indication for short-term increases in the hardness on timescales of less than 1 hr, with the most obvious such increase occurring at $t \approx 37$ hr. Our spectral analysis (§ 4.3) confirms that this hardness increase was accompanied by a temperature increase of the hottest plasma, indicating that the short-term fluctuation at $t \approx 37$ hr was a reheating event.

In contrast, the X-ray light curve during the second observation on 1996 February 13 shows no large-amplitude variability above 3 σ and the count rate is down by an order

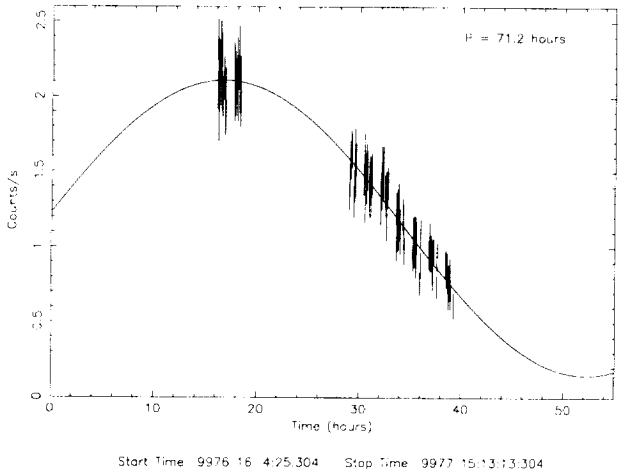

FIG. 3.—Background-subtracted *ASCA* SIS0 light curve of V773 Tau on 1995 September 16–17, binned at 128 s intervals. Error bars are 1 σ. Solid line shows the best fit obtained with a sinusoidal function of the form $A(t) = 1.13 + 0.98$ sin $[2\pi(t - 1.15)/71.2]$ counts s^{-1}. Time is referenced to 0000 UT on 1995 September 16.

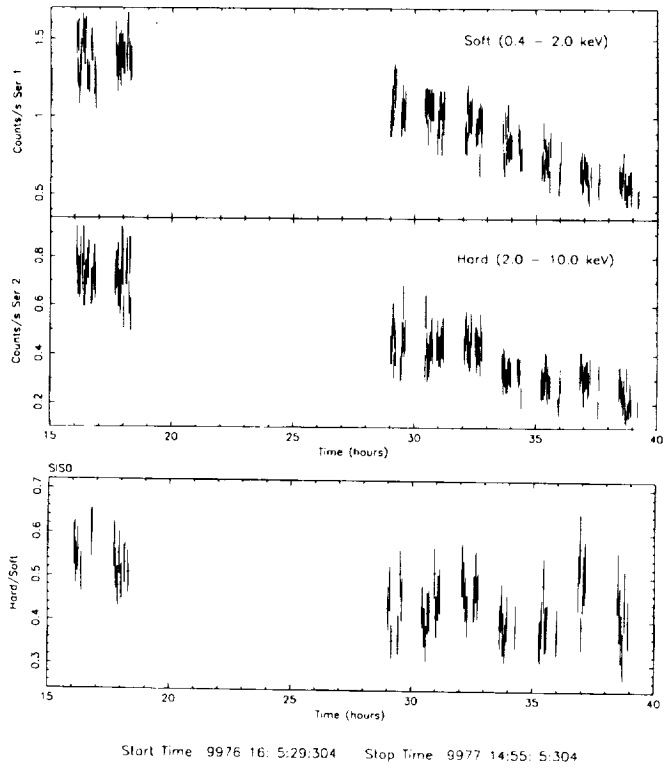

FIG. 4.—Hard- and soft-band SIS0 light curves of V773 Tau on 1995 September 16–17, binned at 128 s intervals. Bottom panel shows the corresponding ratio of hard/soft counts, binned at 256 s. Error bars are 1 σ. Time is referenced to 0000 UT on 1995 September 16.

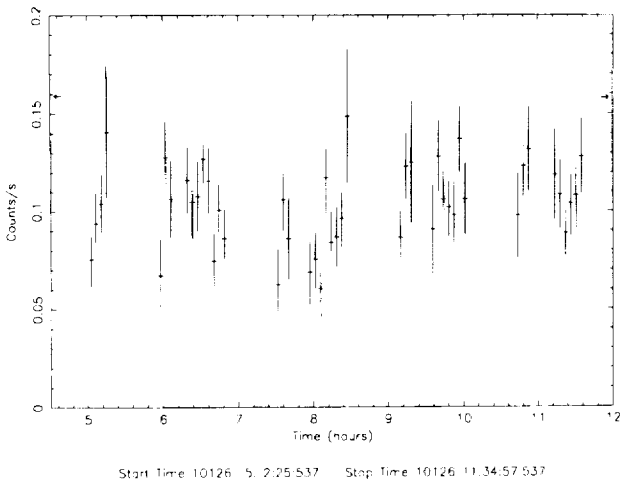

FIG. 5.—Background-subtracted *ASCA* SIS0+SIS1 light curve of V773 Tau on 1996 February 13, binned at 256 s intervals. Error bars are 1 σ. Arrows mark the level of a $+3\ \sigma$ fluctuation. Time is referenced to 0000 UT on 1996 February 13.

of magnitude (Fig. 5). Even so, fits of a constant count rate model to the combined SIS low-state light curves using bin sizes of 128, 256, and 512 s give respective probabilities for a constant count rate of 0.30 (87/81), 0.24 (47/41), and 0.49 (22.5/23), where the quantity in parentheses is χ^2/dof. A Kolmogorov-Smirnov (K-S) test gives lower values $P(\text{const}) \leq 0.18$ when applied to the SIS data. Thus, the possibility of low-amplitude variability cannot be totally dismissed even in this state of reduced activity. The average SIS0 count rate of $0.10 \pm 0.02(1\ \sigma)$ counts s^{-1} is consistent with the value of 0.15 ± 0.13 counts s^{-1} obtained by extrapolating the sinusoidal fit of the 16–17 September light curve to its minimum (Fig. 3). Thus, the reduced SIS0 count rate of 0.10 ± 0.02 counts s^{-1} measured during the 1996 February observation may represent a quiescent level that is always present for this star. It is quite likely that *ROSAT* also caught the star in this state during 1992 September, given the excellent agreement between the *ASCA* low-state flux and that measured by *ROSAT* (§ 4.1). Our spectral analysis indicates that this low state corresponds to an absorption-corrected X-ray luminosity $L_X = 10^{31.09}$ ergs s^{-1} in the 0.5–10 keV band (Table 4).

4.3. *X-Ray Spectra of V773 Tau*

4.3.1. *Methodology and Overview of Results*

Our spectral analysis focuses on the high-resolution SIS spectra shown in Figure 6. The SIS0 and SIS1 spectra from both observations were analyzed using discrete-temperature models within XSPEC (vers. 9.00). For the higher S/N flare spectra acquired on 16–17 September, additional processing was performed. This included construction of the differential emission measure (DEM) distribution and time partitioning of the SIS spectra into six individual segments in order to track the evolution of temperature, emission measure, and flux with time.

XSPEC analysis of the full spectra from 16–17 September allowed us to explicitly determine the neutral hydrogen column density (N_H), the temperature of the X-ray emitting plasma (kT), the volume emission measure (EM),[1] and abundances of metals with prominent emission lines (most notably Fe). Abundances given below were determined using the VMEKAL[2] optically thin plasma code and are referenced to the solar photospheric values listed in Table 2 of Anders & Grevesse (1989). When fitting the spectra with models having more than one temperature component, the abundance of each element was kept the same for all temperature components. The absorption was modeled using cross sections given by Morrison & McCammon (1983).

Time-partitioning of the 16–17 September data set resulted in six individual spectra for each SIS. Each individual spectrum spanned ≈ 0.7–2.5 hr of elapsed time, where the shorter time intervals correspond to segments at the

TABLE 4

SPECTRAL FIT RESULTS FOR V773 TAURI[a]

Parameter	First Pointing[b]	Second Pointing
Date	1995 Sep 16–17	1996 Feb 13
Total counts (SIS0+SIS1)	29904+18950[c]	1297+974[c]
N_H (cm^{-2})	$3.0^{+0.2}_{-0.2} \times 10^{21}$	$[3.0 \times 10^{21}]$
kT_1 (keV)	$0.86^{+0.09}_{-0.09}$	$0.66^{+0.13}_{-0.17}$
kT_2 (keV)	$3.20^{+0.18}_{-0.15}$	$3.20^{+1.60}_{-0.80}$
EM_1 (10^{54} cm^{-3})	$1.44^{+0.42}_{-0.35}$	$0.37^{+0.08}_{-0.09}$
EM_2 (10^{54} cm^{-3})	$9.12^{+0.32}_{-0.41}$	$0.56^{+0.13}_{-0.13}$
EM_2/EM_{total}	0.86	0.65
Fe abundance (× solar)	$0.25^{+0.05}_{-0.05}$	[0.25]
χ^2/dof	508/416	94/129
Flux (10^{-11} ergs cm^{-2} s^{-1})	3.84 (5.31)	0.29 (0.46)
log L_X (ergs s^{-1})	32.01 (32.16)	30.90 (31.09)

[a] From simultaneous fits of *ASCA* SIS0/SIS1 spectra using 2T VMEKAL optically thin plasma model (Mewe et al. 1995) with variable Fe abundance. All other metal abundances were held fixed at the solar values given by Anders & Grevesse 1989. Errors are 90% confidence. Bracketed quantities were held fixed during fitting. Flux and L_X are observed values (0.5–10 keV), followed in parentheses by absorption-corrected values. A distance of 150 pc is assumed.

[b] Emission is variable, quoted values are time-averaged.

[c] Counts were extracted from a circular region of radius 3'.8 centered on the source peak, and include only those counts lying inside the primary CCD (SIS0/CCD1 and SIS1/CCD3). Due to source placement, a significant number of counts fell outside of SIS1/CCD3 and were not recovered.

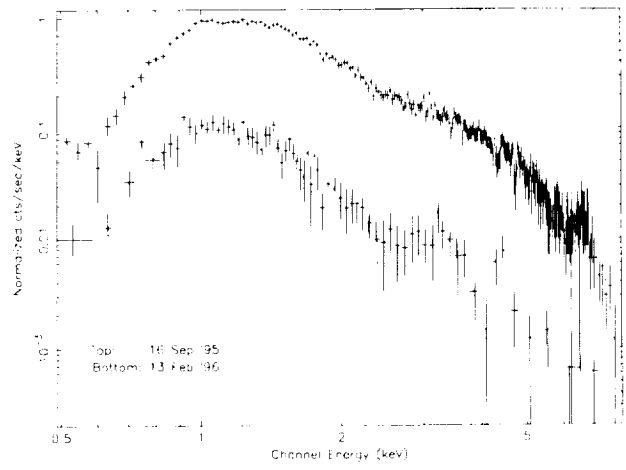

FIG. 6.—Background-subtracted SIS0 spectra of V773 Tau on 1995 September 16–17 (*top*) and 1996 February 13 (*bottom*).

[1] $EM = \int n_e\, n_H\, dV$, where n_e and n_H are the electron and hydrogen number densities and V is the source volume.

[2] The VMEKAL code is based on work by Mewe, Kaastra, & Liedahl (1995) and incorporates recent improvements in Fe L shell atomic physics. This code allows abundances of the following elements to be varied independently: C, N, O, Ne, Na, Mg, Al, Si, S, Ar, Ca, Fe, and Ni.

beginning of the observation when the count rate was highest. Since time-partitioning reduced the S/N (≈2300–4500 counts per SIS per time segment), we were not able to reliably measure N_H or the Fe abundance in the individual spectra. When fitting the individual spectra we held N_H and the Fe abundance fixed at the global best-fit values derived from the full SIS spectra and allowed only kT and EM to vary. Likewise, only kT and EM were varied when fitting the low S/N spectrum acquired on 13 February, holding N_H and the Fe abundance fixed at the best-fit values determined from the 16–17 September SIS spectra.

A more detailed description of the XSPEC and DEM analyses is given below and the main results can be summarized as follows: (1) best fits within XSPEC were obtained with two-temperature optically thin plasma models (Table 4) using metal abundances that are reduced by factors of ≈2–5 below solar, (2) DEM analysis confirms the bimodal temperature structure and shows that almost all of the EM during the flare is due to a hot component whose average temperature is ≈37 million K, (3) the EM of the hot component dropped sharply during the flare decay but the hot-component temperature decreased only moderately from the maximum value of ~42 million K seen at the beginning of the observation (Table 5), and (4) no significant variability was seen in either the temperature or EM of the cool component during the flare decay.

4.3.2. *Discrete Temperature Models*

We have attempted to fit the SIS spectra with a variety of XSPEC models including bremsstrahlung (BREMSS), photon power law (POWERLAW), and an optically thin plasma (MEKAL, VMEKAL). We included an absorption component when evaluating these different models, and during initial fits we held the absorption fixed at the *a priori* estimate $N_H = 3 \times 10^{21}$ cm^{-2}. This estimate was derived from the visual extinction $A_V = 1.37$ (Table 1) and the conversion of Gorenstein (1975). A more precise estimate of the column density that was obtained by allowing N_H to vary in the best-fit VMEKAL model of the high S/N flare spectrum (Table 4) gives $N_H = 3.0\ (\pm 0.2) \times 10^{21}$ cm^{-2}, in excellent agreement with the initial estimate.

The high S/N flare spectra on 16–17 September place tight constraints on the emission mechanism. Bremsstrahlung and power-law models are unable to reproduce the Fe-L shell emission near ~1 keV and are ruled out. Optically thin plasma models that use solar abundances are also unacceptable, even if as many as three temperature components are used. Specifically, a two-temperature (2T) solar-abundance MEKAL model fitted simultaneously to the SIS0/SIS1 flare spectra gives χ^2/dof = 956/417 (χ^2_{red} = 2.29). Adding a third temperature component does not improve this solar-abundance fit significantly.

TABLE 5

PEAK VALUES FOR V773 TAU X-RAY OUTBURST[a]

X-Ray Parameter	Peak Value
Temperature (MK)	42^{+10}_{-5} ($3.6^{+0.9}_{-0.4}$ keV)
Emission measure EM_2 (cm^{-3})	1.5×10^{55}
Count rate (counts s^{-1})[b]	2.6
Flux (ergs cm^{-2} s^{-1})[c]	6.4 (8.7) × 10^{-11}
Luminosity (ergs s^{-1})[c]	1.7 (2.3) × 10^{32}
Energy release (ergs)	$\geq 10^{37}$

[a] Peak values were measured from SIS0 spectra confined to the time interval 1603–1653 UT at the beginning of the observation on 1995 September 16.

[b] SIS0 raw count rate (no correction for PSF).

[c] Observed value in 0.5–10 keV band, followed in parentheses by extinction-corrected value. Distance = 150 pc.

Dramatic improvement in the fit is obtained by allowing metal abundances to vary. If all metal abundances are allowed to vary globally (i.e., all abundances are allowed to deviate equally from their solar values), then a 1T MEKAL model is still unacceptable but a 2T MEKAL model provides an excellent fit and converges to a global abundance of 0.14 (±0.04) solar with χ^2/dof = 440/416 (1.06). Closer inspection using the VMEKAL model (which allows the abundance of each element to be varied independently) shows that the improvement in the fit gained by using non-solar abundances is almost entirely due to the reduced abundance of iron. A 2T VMEKAL model that allows only the iron abundance to vary (along with kT and EM) gives nearly as good a fit as that obtained with a global abundance reduction with χ^2/dof = 508/416 (1.22) and a derived abundance of Fe = 0.25 (±0.05) solar. The best-fit parameters for this variable Fe abundance model are given in Table 4 for both observations, and the corresponding fits are shown in Figures 7 and 8.

Although a 2T VMEKAL model with a reduced Fe abundance does provide a good fit to the SIS spectra, some low-level residuals are present between 1.4–2.2 keV in the flare spectrum (Fig. 7). These residuals can be reduced by allowing Mg, Si, and S to vary along with Fe. In doing so, the derived temperatures and emission measures change very little from the variable Fe abundance values given in Table 4. The fit residuals for a 2T VMEKAL model with variable Fe, Mg, Si, and S abundances are shown in the bottom panel of Figure 7, and this fit converges to Fe = 0.17 (0.11–0.23), Mg = 0.38 (0.15–0.63), Si = 0.52 (0.37–0.68), and S = 0.33 (0.15–0.53) solar with χ^2/dof = 468/413 (1.13).

On the basis of the above analysis, we conclude that the X-ray emission arises in a multitemperature optically thin

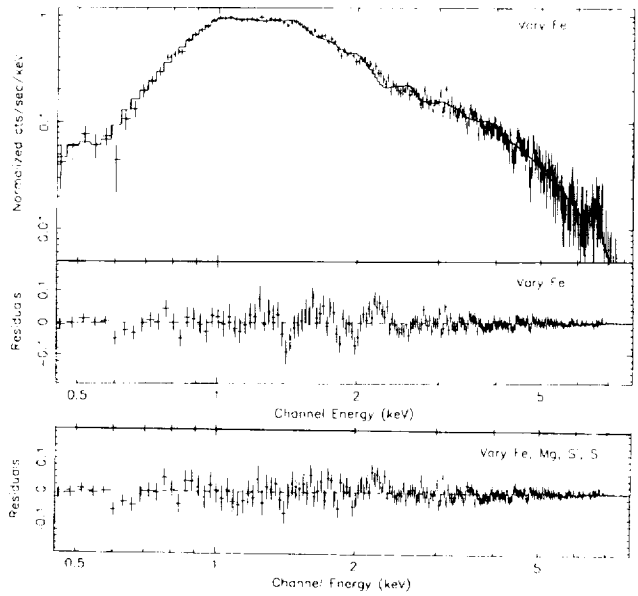

FIG. 7.—Best-fit 2T VMEKAL model of V773 Tau SIS0 spectrum on 1995 September 16–17. Fitted parameters are $kT_1 = 0.8$ keV, $kT_2 = 3.3$ keV, $N_H = 3 \times 10^{21}$ cm^{-2}, and Fe = 0.26 solar. These values differ slightly from those in Table 4, which were obtained by simultaneously fitting SIS0+SIS1 spectra. Bottom panel shows the slightly lower residuals obtained from the same model, but allowing the abundances of Mg, Si, and S to vary along with Fe.

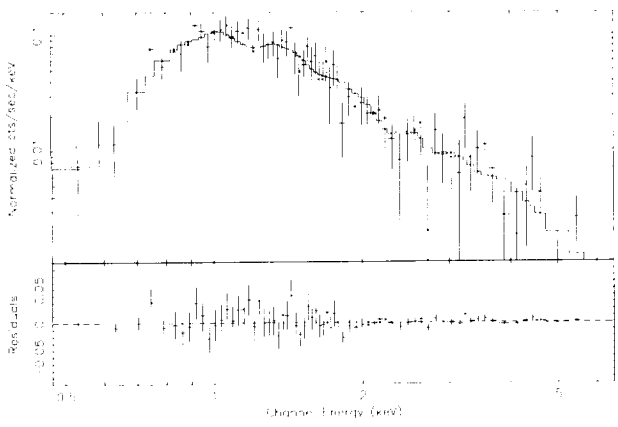

FIG. 8.—Best-fit 2T VMEKAL model of V773 Tau SIS0 spectrum on 1996 February 13. Fitted parameters are $kT_1 = 0.6$ keV, $kT_2 = 2.8$ keV, $N_H = 3 \times 10^{21}$ cm^{-2}, and Fe = 0.25 solar. These values differ slightly from those in Table 4, which were obtained by simultaneously fitting SIS0 + SIS1 spectra.

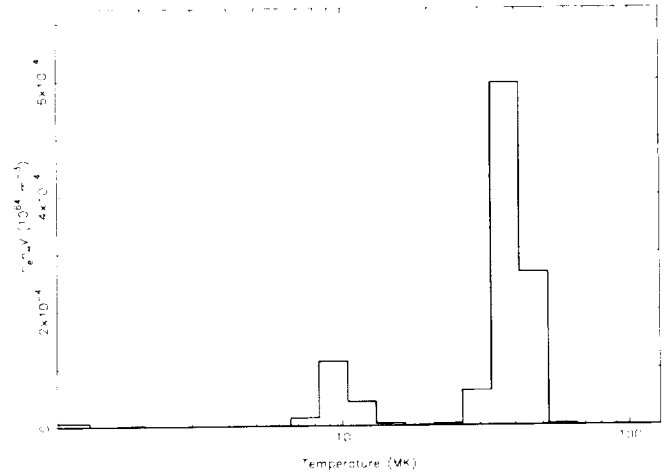

FIG. 9.—DEM distribution of V773 Tau on 1995 September 16–17 as derived from a polynomial algorithm applied to the SIS0 spectrum (see text). The algorithm was applied using a fixed column density $N_H = 3 \times 10^{21}$ cm^{-2} and an iron abundance Fe = 0.25 solar.

plasma with reduced metal abundances. These results are remarkably similar to those derived from high S/N *ASCA* and *EUVE* spectra of other active late-type binaries such as RS CVn systems, as reviewed by Mewe (1996) and White (1996). Our results show that the phenomenon of low metal abundances is not restricted to mature stars on the main sequence and beyond but is also present in magnetically active pre–main-sequence stars. The origin of the metal depletions, which in the case of iron are contrary to trends seen in the solar corona, is not yet understood. It has recently been suggested that coronal density stratification due to hydrostatic equilibrium effects may play a role (van den Oord & Mewe 1997), but one must also be cognizant of the deficiencies in existing plasma codes (Brickhouse et al. 1995; Mewe et al. 1995).

4.3.3. *Differential Emission Measure Models*

The differential emission measure (DEM) function $D(T) = n_e n_H dV/d(\log T)$ measures the relative contribution of plasma at a temperature T to the total spectrum, as described in more detail by Schrijver et al. (1995). We have constructed $D(T)$ for the high S/N SIS0 spectrum from the 16–17 September observation using an iterative polynomial method implemented in the SPEX package (Kaastra, Mewe, & Nieuwenhuijzen 1996b; Kaastra et al. 1996a). The spectra computed by SPEX assume optically thin emission from a plasma in collisional ionization equilibrium, and include both emission lines and continuum contributions (see Mewe et al. 1995 for further details). The polynomial method approximates $\log[D(T)\Delta \log(t)]$ as the sum of n Chebyshev polynomials, as described further in Kaastra et al. (1996a). We included Chebyshev polynomials up to ninth order. The derived DEM distribution shown in Figure 9 was obtained using a fixed column density $N_H = 3 \times 10^{21}$ cm^{-2} and an iron abundance of Fe = 0.26 × solar, as derived from the best-fit 2T VMEKAL models of the SIS0 spectra.

As Figure 9 shows, the DEM of V773 Tau during the outburst is almost entirely dominated by a rather sharply peaked component at $T \approx 37$ MK ($kT \approx 3.2$ keV). Some lower temperature plasma is also present with a maximum contribution near 9 MK (0.8 keV). Although no significant plasma is seen below ≈0.4 keV, one must keep in mind that the SIS detectors are insensitive at these lower energies and we cannot rule out such softer emission on the basis of *ASCA* data alone. The possibility of weak soft emission below 0.3 keV has been mentioned by Feigelson et al. (1994).

Overall, the DEM analysis is in very good agreement with the results from the discrete-temperature VMEKAL model. Both analysis techniques clearly show a bimodal temperature structure with a dominant hot component centered near 3.2 keV and a weaker cool component near 0.8 keV. There is no evidence for plasma at intermediate temperatures of ~1–2 keV (~12–23 million K). Such bimodal distributions have now been inferred from extensive DEM analysis of other young stars such as the solar analog EK Draconis (Güdel et al. 1997).

4.3.4. *Spectral Evolution*

Despite the large difference in X-ray luminosities between the two observations, the time-averaged temperature measurements are the same to within the measurement errors (Table 4). Considering both observations, the 2T VMEKAL model gives average temperatures of $kT_1 = 0.66$–0.86 keV (7.6–10.0 MK) for the cool component and $kT_2 = 3.2$ keV (37 MK) for the hot component. However, some variability in kT_2 was observed during the flare decay on 16–17 September, as discussed below.

In contrast to the rather stable temperature structure, dramatic changes occurred in the emission measure between the two observations and during the flare decay. The total average EM during the flare is a factor of ~11 larger than during quiescence and most of this increase occurred in the hot component EM_2. In addition, the time-averaged fraction of the total EM due to the hot component was larger during the flare (0.86) than in quiescence (0.65). The above comparisons show that the hot plasma component was present not only during the flare but also in quiescence and strongly suggest that some low-level flaring may always be present.

The temperature and EM of both the hot and cool components as a function of time during the flare are shown in Figure 10, along with the total flux profile. These measurements were obtained from simultaneous fits of the time-partitioned SIS0/SIS1 spectra using the 2T VMEKAL

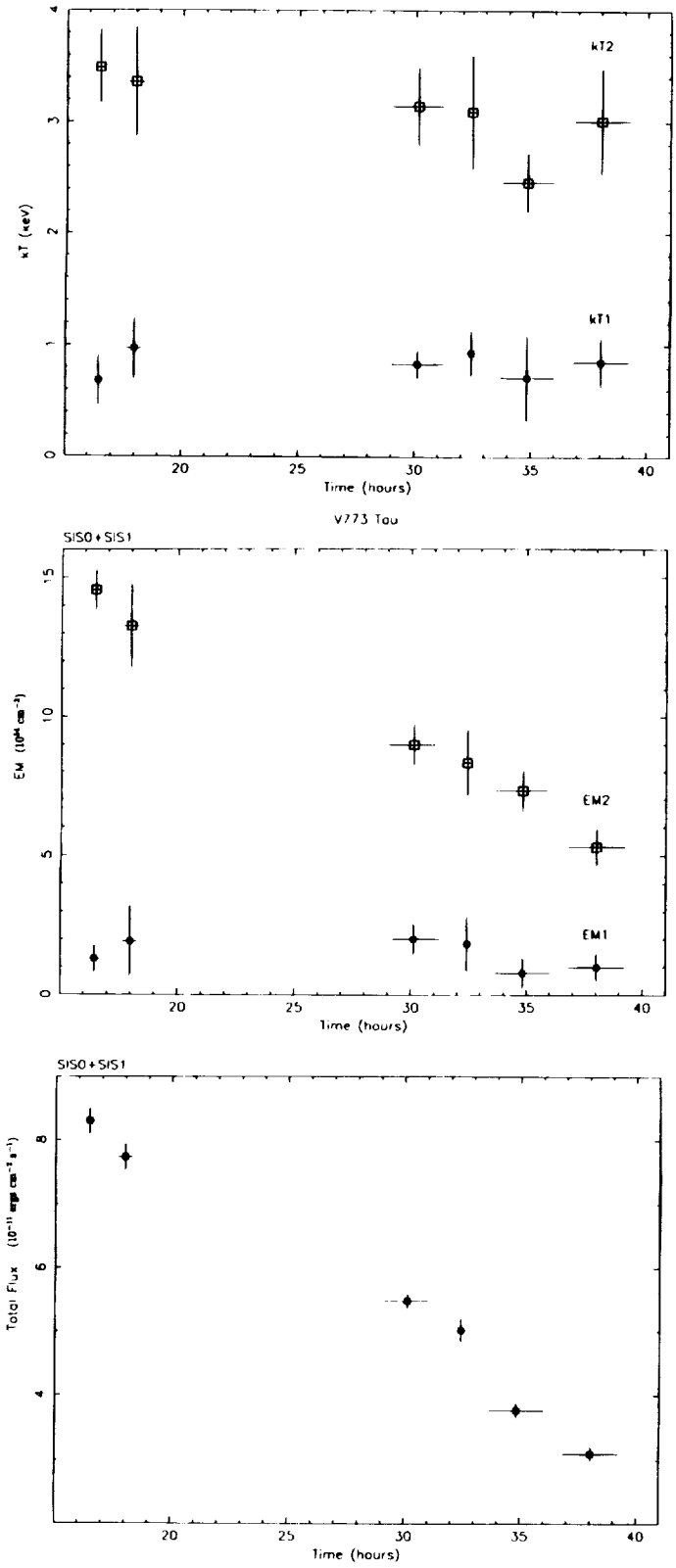

FIG. 10.—Temperature and emission measure distribution of V773 Tau on 1995 September 16–17 as derived from 2T VMEKAL fits of time-partitioned SIS0+SIS1 spectra. Spectral fits use $N_H = 3 \times 10^{21}$ cm^{-2} and a fixed iron abundance Fe = 0.25 solar. Vertical error bars show 90% confidence range and horizontal error bars show time range from which measurement was obtained. Bottom panel is the total extinction-corrected flux.

model, holding the column density and iron abundance fixed at values $N_H = 3 \times 10^{21}$ cm^{-2} and Fe = 0.25 solar. No significant change was detected in either the temperature (kT_1) or emission measure (EM_1) of the cool component during the flare decay. The hot component temperature kT_2 dropped slowly during the first $\sim$21 hr of the observation, falling from $\approx$3.5 to 2.5 keV. However, this trend was reversed $\approx$2 hr prior to the end of the observation when a reheating event occurred, raising the temperature to 3.0 keV. The hot component emission measure EM_2 dropped steadily during the decay and by the end of the observation it had decreased by a factor of $\sim$3 from its initial value. The maximum values of kT_2, EM_2, and total flux all occurred during the first time partition centered at $t = 16.47$ hr and the peak flare values are given in Table 5.

The time-partitioned spectra clearly show that the flare-like variability is associated with the hot plasma component. The slow decline in the X-ray light curve is mimicked by a strong decline in the emission measure of the hot component but only a modest drop in temperature. The sharp drop in EM_2 reflects either a drop in the average electron density or a reduction in the visible volume.

4.4. *X-Ray Properties of IRAS 04113+2758 and Anon 1*

Before considering specific variability models for V773 Tau, we summarize the *ASCA* results for IRAS 04113+2758 and Anon 1 (Table 3). IRAS 04113+2758 is of particular interest since it is a strong class II IRAS source that is quite likely a young binary system. It appears double in near-IR images with a component separation of 3.″5, the southeast component being about a factor of 2 brighter at *K* band than its companion (Kenyon et al. 1990; Tamura et al. 1991). Thus, the X-ray emission could be the superimposed contribution of these two objects. A strong CO outflow has been detected (Moriarty-Schieven et al. 1992), but higher angular resolution observations will be needed to show conclusively that it is driven by IRAS 04113+2758.

The GIS light curve in Figure 11 shows that the X-ray emission of IRAS 04113+2758 is variable on a timescale of a few hr. Because of the low signal-to-noise ratio, it is not clear if the increase in count rate observed at $t \approx 9$ hr was impulsive or gradual. Spectral information is incomplete

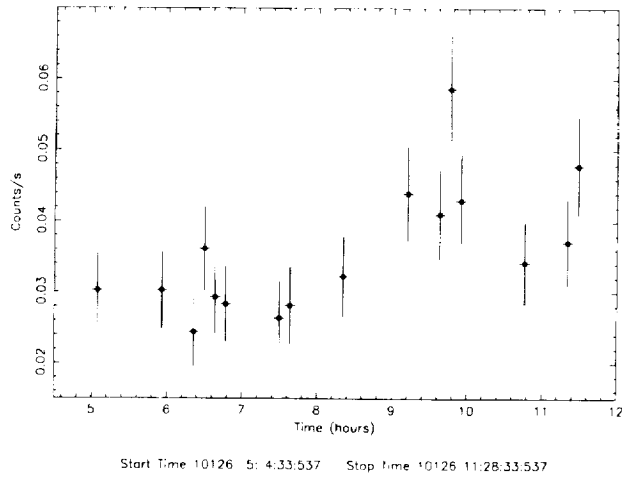

FIG. 11.—Background-subtracted GIS2+GIS3 light curve of IRAS 04113+2758 on 1996 February 13, binned at 512 s intervals. Error bars are 1 σ. Time is referenced to 0000 UT on 1996 February 13.

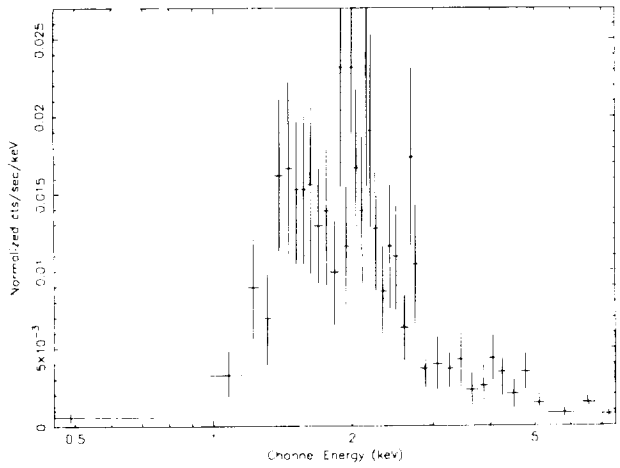

FIG. 12.—Background-subtracted GIS2 spectrum of IRAS 04113+2758 on 1996 February 13. The spectrum contains 389 net counts and has been rebinned to a minimum of 10 counts per energy bin. The GIS2 detector is not sensitive below ≈ 0.8 keV.

since this source fell outside of the SIS field of view and the GIS do not provide coverage below ≈ 0.8 keV. However, significant counts are seen in the GIS spectra up to energies of ~ 3–4 keV (Fig. 12). Fitting the GIS2/GIS3 spectra simultaneously with a solar-abundance 1T MEKAL model gives a temperature $kT = 3.1$ [2.6–3.6] keV, and a bremsstrahlung fit gives similar values. At a distance of 160 pc (Kenyon et al. 1990) the flux measured from GIS fits (Table 3) gives $L_X = 7 \times 10^{30}$ ergs s^{-1} (0.8–10 keV), which is uncorrected for absorption since the GIS spectrum does not tightly constrain N_H.

Anon 1 is a nebulous weak-lined TTS of spectral type M0 V (Herbig & Bell 1988). Its estimated age is ~ 2 Myr and the stellar luminosity is $L_* = 0.77\ L_\odot$ (Martín et al. 1994). The SIS and GIS light curves show no evidence for X-ray variability down to a time resolution of 512 s. Fitting the SIS spectra (≈ 370 net counts per SIS) with a one-temperature solar abundance MEKAL model gives $kT = 3.5$ [2.4–5.9] keV and a best-fit hydrogen column density $N_H = 2.1 \times 10^{21}$ cm^{-2}. This value of N_H is in good agreement with that estimated from $E(B-V)$ using the photometry of Martín et al. (1994), assuming a normal extinction law. The 1T MEKAL fit improves slightly by allowing the global abundance to deviate from solar, converging to a value of 0.38 solar and a lower temperature $kT = 3.0$ [2.1–5.1] keV. We have investigated 2T MEKAL models but find no significant fit improvement over the 1T MEKAL model and are thus unable to provide a temperature estimate for the cooler component (≤ 1 keV) that is usually detected in WTTS. The fluxes obtained from 1T MEKAL fits (Table 3) give an extinction-corrected luminosity $L_X = 8 \times 10^{30}$ ergs s^{-1} (0.5–10 keV) at an assumed distance of 160 pc.

In summary, both IRAS 04113+2758 and Anon 1 show evidence for hot plasma at temperatures of ~ 3 keV, comparable to the hot component seen in V773 Tau and other active late-type stars. The most interesting behavior revealed in these two weak detections is the variability of IRAS 04113+2758. More sensitive observations of this infrared double over a longer time interval are warranted to determine if the variability exhibits any systematic behavior.

5. DISCUSSION: FLARE MODELS AND THE VARIABILITY OF V773 TAURI

We now examine several different models that could potentially explain the slow variability seen during the V773 Tau outburst. The origin of the variability is of considerable interest since it clearly differs from the solar-like flare behavior that is often seen in T Tauri stars and that is characterized by an impulsive rise phase followed by a near-exponential decay over a period of a few hr (e.g., DD Tau, shown in Fig. 4*a* of Strom & Strom 1994). X-ray flares with long decay times that may be more akin to that observed here have been detected in the young star P1724 (Gagné, Caillault, & Stauffer 1995; Preibisch, Neuhäuser, & Alcalá 1995) and in the RS CVn binaries HR 5110 (Graffagnino, Wonnacott, & Schaeidt 1995) and CF Tuc (Kürster & Schmitt 1996).

Several mechanisms could be listed as candidates for explaining the slow variability of V773 Tau. These include (1) a slowly decaying flare, (2) rotational modulation of the X-ray emitting region, (3) an eclipse of the active star, (4) slowly varying absorption, and (5) modulated accretion. Of these possibilities, only the first two seem plausible. The orbital inclination of V773 Tau is probably not high enough to produce eclipses (Welty 1995). Furthermore, there is no gradual increase in the hardness ratio during the observation (Fig. 4), contrary to what would be expected if the falloff in count rate were due to a slow increase in absorption. Modulated accretion could give rise to a periodic light curve that varies at a beat frequency equal to the difference between the stellar rotation frequency and the magnetospheric orbital frequency (Smith, Bonnell, & Lewis 1995). However, the variability detected here seems to be locked to the stellar rotation frequency and is thus not a beat phenomenon.

We thus focus on flare decay models and discuss the implications of rotational modulation. In reality, we believe that both flare decay and rotational effects are involved and that the observed variability is due to progressive occultation of the flaring region via stellar rotation. Although the sinusoidal shape of the light curve can be most readily explained as a rotational effect, several lines of evidence indicate that these dynamical effects are superimposed on the cooling phase of a large flare. Direct evidence for flare emission includes (1) the extremely high L_X (being a factor of ~ 13 larger than measured in the follow-up observation), (2) a decrease in the light curve hardness ratio early in the observation (Fig. 4), and (3) a slow but discernible decrease in the hot-component temperature during all but the last few hours of the observation (Fig. 10).

In the following, we compare the observed decay with that predicted by two well-known flare decay models that are based on the solar analogy, namely the quasi-static cooling loop model and the two-ribbon flare model. We then briefly consider the relevance of interbinary flares and flares due to star-disk magnetic interaction. Finally, we investigate the implications of rotational modulation.

5.1. *Solar-like Flare Models*

5.1.1. *Quasi-static Cooling Loops*

The quasi-static cooling loop model assumes that the hot flaring plasma is confined to coronal loops that cool radiatively through states of constant pressure, emitting thermal X-rays in the process (van den Oord, Mewe, &

Brinkman 1988; van den Oord & Mewe 1989, hereafter vdOM89). This model can only be applied during the decay phase of a flare when *both* temperature and emission measure are decreasing. Although it is clear from Figure 10 that EM_2 decreased steadily during the V773 Tau observation, the interval(s) over which kT_2 decreased are less obvious because of the temperature uncertainties. However, one can reasonably argue for a slow temperature decrease during all but the last ≈ 3 hours of the observation, at which time reheating probably occurred.

If the cooling is quasi-static then the ratio $R = T_2^{3.25}/EM_2$ should be constant (eq. [27] of vdOM89). This ratio is plotted in Figure 13 for all six (kT_2, EM_2) measurements obtained from the time-partitioned SIS spectra. Although the uncertainties are large, the first five measurements are consistent with a constant value $\bar{R} = 0.57$ (0.28–0.85). However, the sixth measurement centered at $t = 38.02$ hr shows a large upward fluctuation with a value $R = 1.10$ (0.65–2.23), suggesting that the quasi-static cooling assumption is not valid during the last ≈ 3 hours of the observation. This upward fluctuation in R overlaps the increase in hardness ratio seen at $t \approx 37$ hr, adding further support to the hypothesis that the plasma was reheated.

We thus proceed under the assumption that the quasi-static cooling model may apply during all but the last ≈ 3 hr of the observation. We then ask if the simplest form of the model, which assumes no additional heating during the decay, can explain the observations prior to the last (kT_2, EM_2) measurement. In the absence of additional heating, the quasi-static model predicts that the temperature (T), electron density (n_e), and radiative energy (E_r) should decay with time as $[1 + (t/3\tau)]^{\beta}$, where τ is a time constant to be determined from the observations. From Table 5 of vdOM89 the predicted power-law exponents are $\beta = -8/7$ (T), $\beta = -13/7$ (n_e) and $\beta = -4$ (E_r). Under the assumption of constant loop volume, the emission measure decay should be of the same form with $\beta = -26/7$ (EM).

We have fitted the observed decay profiles of kT_2, EM_2, and X-ray flux (subtracting the constant quiescent contribution) with the above model, leaving τ as a free parameter. This fit was applied to the first five independent measurements from the time-partitioned SIS spectra, excluding the sixth measurement for the reasons discussed above. Since the decay was already in progress at the beginning of the observation, each fit was normalized to the first measurement centered at $t = 16.47$ hr.

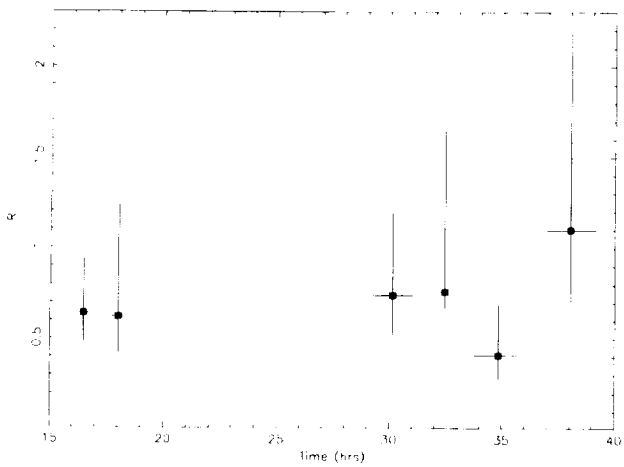

FIG. 13.—Ratio $R = T_2^{3.25}/EM_2$ for V773 Tau on 1995 September 16–17, where T_2 is in units of 10^7 K and EM_2 in units of 10^{53} cm^{-3}. Values of T_2 and EM_2 were obtained from 2T VMEKAL fits of time-partitioned SIS0+SIS1 spectra (see Fig. 10).

The best overall fit to the three decay profiles was obtained for $\tau \approx 30.5$ hr, and Figure 14 shows this best fit. For comparison, we have also overlaid the best-fit energy release profile ($\beta = -4$) on the X-ray light curve, renormalized to the maximum count rate. As can be seen, the model provides a good fit of the EM_2 decay. Also, the predicted kT_2 decay profile is in reasonably good agreement with the data but the fit residuals do increase toward later times. On the other hand, the model does not provide a satisfactory fit of the flux profile, and this discrepancy is more apparent when the model is overlaid on the light curve. The decline in flux and count rate in the post-gap segment ($t \geq 29$ hr) is much steeper than predicted by the model and the convex shape of the light curve is in conflict with the concave structure of the model.

The above discrepancies show that the simplest implementation of the quasi-static cooling loop model does not explain the observed energy release profile. One suspects that if this model applies at all, then the physical situation in the flaring region is considerably more complex than assumed here. Factors that may be relevant and that could invalidate the model include (1) additional heating during the decay phase, either from a discrete event in the data gap that went undetected or from quasi-continuous low-level flaring; (2) complex loop geometry, including multiple flaring loops with different cooling curves; and (3) dynamic effects such as stellar rotation that may be superimposed on the intrinsic loop emission profiles.

5.1.2. *Two-Ribbon Flares*

The large energy release and slow decay of the V773 Tau outburst are reminiscent of solar two-ribbon flares. The two-ribbon flare model is described by Kopp & Poletto (1984) and has been applied to long-duration stellar flares in several cases (cf. Poletto, Pallavicini, & Kopp 1988). This model attributes the flare energy release to magnetic reconnection of an entire arcade of coronal loops, a fraction of this energy escaping at X-ray wavelengths.

The key parameter in this model is the neutral point, whose height $y(t)$ increases with time. The neutral point is, more precisely, a neutral current sheet formed by the reconnection of magnetic field lines converging from opposite sides, with the most recently formed coronal loops lying just below the neutral sheet. At heights below the neutral point, the magnetic field is assumed to be dipolar and azimuthally symmetric with a latitudinal dependence that is described in terms of Legendre polynomials $P_n(\theta)$. Above the neutral point, the magnetic field is assumed to be radial.

The theoretical model makes contact with observations through the energy release per unit time, which is predicted to be (eq. [3] of Kopp & Poletto 1984)

$$\frac{dE}{dt} = \frac{dE}{dy}\frac{dy}{dt} = -R_*^3 B^2 G(n) \frac{y^{2n}[y^{2n+1} - 1]}{[n + (n+1)y^{(2n+1)}]^3} \frac{dy}{dt}, \quad (1)$$

where

$$G(n) = \frac{1}{8\pi} 2n(n+1)(2n+1)^2 I_{12}(n). \quad (2)$$

In the above, B is the magnetic field strength at the stellar surface on the axis of symmetry (latitude $\theta = 0°$, 180°), and

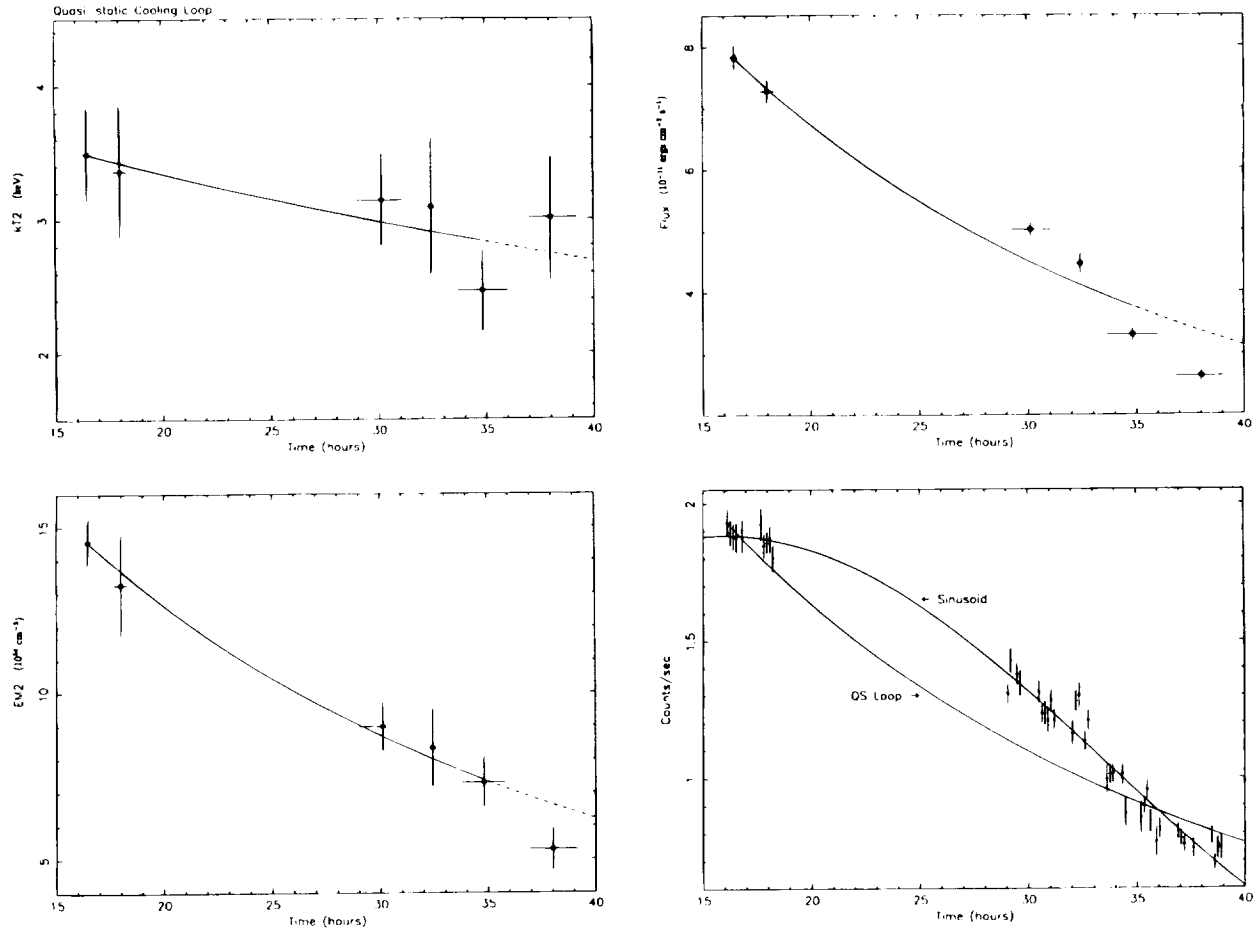

FIG. 14.—Best-fit of a quasi-static cooling loop model (*solid line*) to the V773 Tau decay profile on 1995 September 16–17. Model is extrapolated to the last data point (*dashed line*), which was not included in the fit because of suspected reheating. The model assumes no additional heating and uses a decay timescale of $\tau = 30.5$ hr (see text). Observed data points (*solid squares*) were derived from fits of time-partitioned SIS0+SIS1 spectra using a 2T VMEKAL model with the iron abundance fixed at Fe = 0.25 solar and the column density fixed at $N_H = 3 \times 10^{21}$ cm^{-2} (see text). The quiescent contribution has been subtracted from the extinction-corrected flux. Vertical error bars are 90% confidence ranges, and horizontal error bars show the time range over which the measurement was obtained. For comparison, a sinusoid of period 71.2 hr has been overlaid on the light curve.

$I_{1,2}(n)$ is a constant whose value depends on the degree n of the Legendre polynomial (eq. [2] of Kopp & Poletto 1984).

On the basis of solar flare observations, the height of the neutral point is assumed to increase with time according to (eq. [7] of Poletto et al. 1988)

$$y(t) = 1 + \left(\frac{H_{\max}}{R_*}\right)\left[1 - \exp\left(-\frac{t}{\tau}\right)\right]. \qquad (3)$$

The maximum height of the neutral point is not deducible from the theory and is usually assumed to be equal to the latitudinal extent of the flaring region, that is $H_{\max} \approx (\pi/n)R_*$. The shape of the energy release profile is primarily determined by the time constant τ, which is varied to obtain the best fit to the observed energy release profile. The polynomial degree n can also be varied, but for a given τ the energy release curves for different n are quite similar during the decay phase (cf. Fig. 13 of Kürster & Schmitt 1996). Similarly, the field strength B can be varied to achieve normalization, but it is not of primary interest here since we are concerned with time dependence.

Figure 15 shows the energy release profile predicted by equation (1) for a representative case with $n = 5$ and two different decay timescales. The two-ribbon model is over-

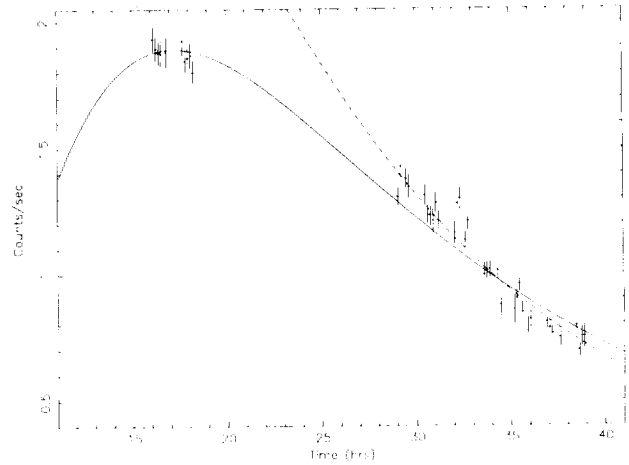

FIG. 15.—Two-ribbon flare model with polynomial degree $n = 5$ (eq. [1]) overlaid on the averaged SIS0+SIS1 light curve for V773 Tau on 1995 September 16–17. Solid line is for decay timescale $\tau = 63$ hr, normalized to count rate at beginning of observation. Dashed line is for $\tau = 50$ hr, normalized to count rate in post-gap segment ($t \geq 28$ hr). Light curve is binned to 512 s intervals.

laid on the SIS light curve and the model normalization and time of maximum intensity (flare peak) were treated as adjustable parameters. The solid line shows a fit with $\tau = 63$ hr, normalized to match the count rate at the beginning of the observation. As can be seen the fit is satisfactory during the first few hours of the observation, but the model decay is too slow at later times. The model shown by the dashed line attempts to remedy this by using a faster decay of $\tau = 50$ hr, normalized to match the count rate in the post-gap segment ($t \geq 28$ hr). The fit in the post-gap segment is indeed much better, but this model seriously overestimates the count rate when extrapolated backward to the beginning of the observation. These representative fits show that the two-ribbon model has difficulty reproducing the strong convex curvature in the *ASCA* light curve. Because of the relative insensitivity of the decay profile to the polynomial degree n, this deficiency cannot be removed by using a different value of *n*.

5.2. *Unconventional Flare Models*

5.2.1. *Interbinary Flares*

Slowly decaying X-ray flares in some RS CVn binary systems such as HR 5110 have been attributed to magnetic reconnection between the two binary components (Graffagnino et al. 1995). Magnetic interaction has also been postulated to explain a large ultraviolet flare in the RS CVn binary UX Ari (Simon, Linsky, & Schiffer 1980). Because of the strong empirical similarities between WTTS and RS CVn systems, we ask whether the V773 Tau X-ray outburst could have been due to binary interaction. This is an interesting possibility, but it is more difficult to justify for V773 Tau because of its wider component separation $a = 73.4\ R_\odot$ (Welty 1995), which is a factor of ~ 5–7 times larger than the RS CVn binaries mentioned above.

There is very little theoretical framework for discussing interbinary flares in T Tauri stars. The situation is obviously complex since an interbinary loop or filament will be subject to the combined Lorentz and mechanical forces of both stars. Stationary coronal loop models developed for single solar-like stars (e.g., Serio et al. 1981) may be of little relevance in the complicated gravitational and magnetic fields between two T Tauri stars. Consequently, we will confine our discussion to a few brief remarks.

From the standpoint of energetics, an interbinary flare does look favorable. As discussed by van den Oord (1988), the energy stored in an interbinary filament of characteristic length $2\mathscr{L}$ is $W = \mathscr{L}(0.5\ a\ B_{\rm surf})^2$, where $B_{\rm surf}$ is the magnetic field strength at the stellar surface. If the field strength is comparable to the value $B_{\rm surf} \sim 1$ kG that has been estimated for other WTTS (Basri, Marcy, & Valenti 1992), then one obtains $W \sim 10^{43}$ ergs for a hypothetical interbinary loop in V773 Tau. This is more than adequate to account for the observed X-ray energy release ($\sim 10^{37}$ ergs).

In spite of the favorable energetics, there are potential problems with the interbinary picture. To initiate reconnection with the companion, a loop or filament would need to extend well into the interbinary region. Taking the height of such a representative loop to be $H \approx a/2$ and expressing this in terms of the pressure scale height(s) H_p, one obtains $H \approx 2.7$–$4.5\ H_p$, where $H_p = 3.4R_*$ for the K5 component and $H_p = 5.7R_*$ for the K2 component (eq. [3-276] of Lang 1980). Such long loops are already at the edge of (or possibly outside of) the stability envelope for single solar-like stars (Serio et al. 1981), and it is not at all clear that they could be maintained under the additional perturbative forces of a binary companion.

Estimates of the loop electron density and volume can be extracted from the *ASCA* flare light curve and the observed flare emission measure EM_2. For a loop that is cooling radiatively, the electron density is related to the radiative cooling timescale τ_r (eq. [10] of vdOM89). To obtain an estimate of τ_r we consider the post-gap segment of the light curve, which can be roughly modeled as an exponential decay with an *e*-folding time $\tau_r \approx 12$ hr (§ 4.2). If this post-gap segment represents the radiative cooling phase of a loop of average temperature ≈ 37 MK, then the inferred loop electron density is $n_e \approx 2 \times 10^{10}$ cm^{-3} (eq. [10] of vdOM89) and the corresponding pressure is $P = 2n_e kT \approx 200$ dyn cm^{-2}. Using the observed value of EM_2 and the relation $EM = n_e^2 V$, the inferred emitting volume is then $V \approx 2 \times 10^{34}$ cm^3, or equivalently $V \approx V_*$. By comparison, the volume between the two stars is $V_{K-K} \sim 23V_*$, where we have approximated the interbinary volume as a cylinder with a length equal to the semimajor axis and a diameter $2R_*$. Thus, the flaring plasma would occupy only about 4% of the interbinary volume.

The pressure $P \approx 200$ dyn cm^{-2} is uncomfortably large for a long loop of interbinary dimensions ($L \sim a \sim 10^{12}$ cm), being an order of magnitude larger than predicted for loops of similar length and temperature in single solar-like stars (Fig. 1 of Maggio & Peres 1996). Also, these high pressures lead to inferred surface magnetic field strengths that are extreme. Assuming equipartition $B^2/8\pi \approx P$, a minimum magnetic field strength $B_{\rm min} \sim 70$ G is needed for plasma confinement. In order to sustain such a field at a distance of $\sim 15R_*$ (i.e., at the midpoint between the two stars), then a surface field $B_{\rm surf} \approx 15$ kG is needed assuming a slow falloff $B(r) \propto r^{-2}$ and a much larger surface field is obtained using the dipolar form $B(r) \propto r^{-3}$. The inferred value $B_{\rm surf} \gtrsim 15$ kG is an order of magnitude larger than estimates for other WTTS (Basri et al. 1992).

Because of the above concerns about the stability of long loops, high loop pressures, and magnetic confinement in the interbinary region, we cannot argue strongly for the interbinary flare picture in V773 Tau. Clearly, extension of existing theoretical work on loop structure and stability in single solar-like stars to binary configurations would be useful. Although interbinary reconnection may occur in more closely spaced systems during strong flares, recent X-ray observations of the eclipsing RS CVn system AR Lac ($a = 9.2\ R_\odot$) during periods of low activity have failed to detect hot interbinary plasma (Ottmann, Schmitt, & Kürster 1993; see also White et al. 1994).

5.2.2. *Flares from Star-Disk Magnetic Reconnection*

There is little doubt that V773 Tau has a magnetosphere, as has been clearly shown in the VLBI study of Phillips et al. (1996). If V773 Tau is also surrounded by a disk, then the stellar magnetic field may interact with the disk. In the model of Ghosh & Lamb (1979), the stellar field lines thread parts of the disk that rotate at angular velocities different from the star, causing the field to wind up. Subsequent shearing and reconnection of the magnetic loops would result in intense releases of magnetic energy, accompanied by rapid heating and thermal X-ray emission. We cannot yet answer the question of whether this mechanism might have caused the V773 Tau X-ray outburst since the theory

of star-disk interaction in T Tauri stars is still evolving. We thus restrict our discussion to new developments that bear directly on this issue and that reduce the need to invoke this process in V773 Tau.

First, we note that Shu et al. (1994) have recently proposed a picture describing the interaction of a T Tauri star with its disk that differs in several respects from the Ghosh & Lamb model. Most importantly, in the Shu et al. picture the stellar magnetic field only intersects the disk at the corotation radius. Outside of that radius, the field is excluded from the disk by shielding currents that are set up in the conducting disk surface. Inside the corotation radius the field maintains a fixed pattern that rotates with the star. Thus, in the Shu et al. picture the field does not wind up, and if this model is correct then there is no need to invoke star-disk reconnection.

Second, a disk is obviously needed to justify any discussion of star-disk interaction, and the arguments in favor of a disk around V773 Tau are less than compelling. Beckwith et al. (1990) detected 1.3 mm continuum emission from V773 Tau at a flux $F_{1.3\,\mathrm{mm}} = 42(\pm 6)$ mJy, and under the assumption that the emission was thermal, they derived a disk mass of 0.01 $M_\odot$. However, a follow-up observation several years later gave a lower value $F_{1.3\,\mathrm{mm}} = 24(\pm 4)$ mJy (Osterloh & Beckwith 1995). Under the assumption of thermal disk emission ($F_\nu \propto \nu^\alpha$, $\alpha \geq 2$), the expected 800 μm flux would then be greater than 63 mJy, which is in conflict with the upper limit $F_{0.8\,\mathrm{mm}} \leq 29$ mJy (3 σ) obtained by Jensen, Mathieu, & Fuller (1996). Suspicions that the millimeter flux of V773 Tau might be variable have now been confirmed in recent interferometer observations that show the 2.7 mm flux dropping from 30 mJy to an undetectable level (≤ 3 mJy) in less than six months (Dutrey et al. 1996). This strong variability indicates that the millimeter emission is dominated by a nonthermal component, confirming an earlier suggestion by Skinner, Brown, & Walter (1991). Although the presence of nonthermal millimeter (and centimeter) emission does not in itself rule out the existence of a disk around V773 Tau, it does indicate that the disk mass derived from previous 1.3 mm observations may be a serious overestimate. The 800 μm upper limit obtained recently by Jensen et al. yields a disk mass below 0.001 $M_\odot$, suggesting that if a disk exists at all then it is tenuous.

Even if V773 Tau does have a disk, any star-disk magnetic interaction may be suppressed by dynamical clearing of the inner disk region. A close binary system is expected to rapidly truncate both circumstellar and circumbinary disks and more extensive gap clearing is expected for eccentric orbits. Observational evidence for this effect may have recently been found by Jensen et al. (1996), who showed that the submillimeter emission of close T Tauri binaries ($a \leq 50$ AU) is significantly weaker than that of wider binaries or single T Tauri stars. This behavior is observed down to separations of a few AU but it is not known whether the trend continues to smaller separations of less than 1 AU due to sample limitations. Even so, one suspects that clearing of the innermost disk region in V773 may have been extensive due to its tight eccentric orbit ($a = 0.343$ AU, $e = 0.27$). The third near-IR component at an offset of 0".11–0".17 may have also played a role in disk clearing if it is physically associated with V773 Tau.

5.3. *Rotational Modulation*

We now proceed on the assumption that the slow light curve variability on 16–17 September is due to rotational modulation of the region associated with the X-ray flare. Arguments in favor of a rotational interpretation are the following: (1) a best-fit sinusoidal structure with an inferred X-ray period of 2.97 days, which is in good agreement with the optical rotation period(s) of the two K-type components; (2) a predicted minimum count rate from the sinusoidal fit of 0.10 ± 0.02 counts s^{-1}, which is consistent with the quiescent count rate observed on 1996 February 13; and (3) a rapid drop in the emission measure of the hot component, which is accompanied by very little change in the observed temperature, suggesting progressive obscuration of the emitting volume.

Since our data provide no information on the rise phase, we assume that the light curve rise and decay were symmetric, giving a sinusoidal "bump." We then use the light curve analysis technique developed by Güdel & Schmitt (1996) to derive an upper limit on the volume of the region responsible for the modulation, and thus a lower limit on the electron density n_e. Extrapolation of the light curve in Figure 3 backward in time under the assumption of symmetry implies that the modulating source(s) would have been visible for at least ≈ 46 hr (phase interval = 0.65 for $P_{\mathrm{rot}} = 71.2$ hr), and *invisible* over a phase interval = 0.35. For an assumed stellar inclination $i \approx 90°$, one then obtains an upper limit on the volume occupied by the modulating source of $V_{\mathrm{inv}} \approx 0.03 R_*^3$ (Fig. 2 of Güdel & Schmitt 1996). This upper limit, along with the observed value of EM_2 (Table 4), gives a lower bound $n_e \geq 2 \times 10^{11}$ cm^{-3}.

Adopting the lower limit $n_e = 2 \times 10^{11}$ cm^{-3} leads to some interesting conclusions regarding energy input and geometry. First, we note that if the hot ≈ 37 MK plasma is magnetically confined and in pressure equilibrium then this lower limit on n_e requires a magnetic field strength $B \geq 240$ G. Second, the radiative loss timescale for a ≈ 37 MK plasma at this density is only ≈ 1.5 hr (eq. [10] of vdOM89). In contrast, the temperature decay timescale is at least an order of magnitude larger (Fig. 10). This apparent discrepancy implies that if the light curve variability is due to rotational modulation, then the hot high-density plasma in the region responsible for the modulation must be reheated nearly continuously. We have in fact already argued for reheating on other grounds (§§ 4.2 and 4.3).

Using the lower limit $n_e = 2 \times 10^{11}$ cm^{-3} and making some basic assumptions about loop geometry leads to constraints on coronal loop heights. Assuming that the region containing the hot plasma consists of N identical semicircular coronal loops of height H above the stellar surface, then loop height and emission measure are related by (eq. [3] of vdOM89, with $L = \pi H$)

$$\mathrm{EM} \approx (\pi^4/8) n_e^2 H^3 (1 + \Gamma)(N\alpha^2) . \quad (4)$$

Here the aspect ratio α is the ratio of the loop base diameter to loop length L, where $\alpha \approx 0.1$ in the solar case (Golub et al. 1980). The expansion factor Γ is the ratio of the loop cross-sectional area at the loop top to that at the base, where typical values are $\Gamma \approx 1$–10 (Mewe et al. 1997).

Figure 16 shows the loop heights derived from equation (4) using the observed hot-component emission measure EM_2. A single loop of constant cross section ($N = 1$, $\Gamma = 1$) would have a height $H = 0.58 R_*$. This value is less than the pressure scale heights $H_p \approx 3.4$–$5.7\ R_*$ of the K5 and K2 stars, so loop hydrodynamic stability criteria would not be violated. For a loop of this height to be *completely* occulted

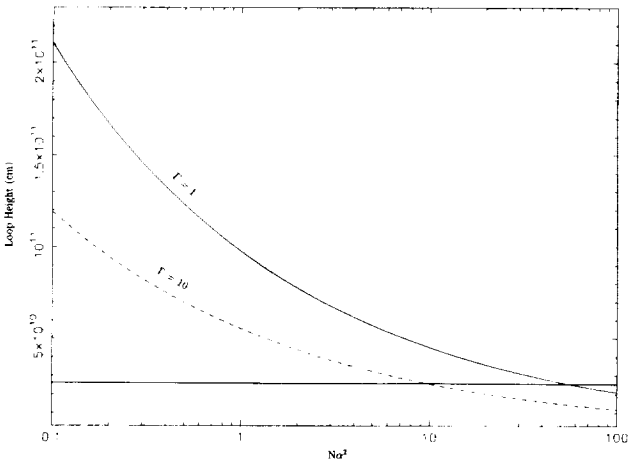

FIG. 16.—Coronal loop height H as a function of $N\bar{\alpha}^2$, where N is the number of loops and $\bar{\alpha} = \alpha/0.1$, where α is the aspect ratio (see text). Horizontal solid line shows the maximum loop height that can be totally occulted at latitude 60° for a stellar inclination $i = 90°$. H has been computed using eq. (4) with $n_e = 2 \times 10^{11}$ cm^{-3} and an emission measure $EM_2 = 9.1 \times 10^{54}$ cm^{-3}.

by rotation it must lie at a latitude below $\theta_{max} = 40°$. A single expanding loop with $\Gamma = 10$ has a height $H = 0.33\ R_*$ and would be totally occulted below a latitude $\theta_{max} = 49°$. Here we have used the relation[3]

$$\sin \theta_{max} = [1 + (H/R_*)]^{-1} . \quad (5)$$

One could attempt to extract more precise information on the spatial location of the region responsible for the modulation by attempting to reconstruct the *ASCA* light curve using a variety of mapping techniques, as described by Schmitt (1996). However, such techniques often lead to nonunique solutions even when complete light curve information is available, and we thus believe that such detailed modeling would be premature given that our data do not span a full rotation cycle and do not provide rise-time information. We will thus resist the temptation to overinterpret the data and restrict ourselves to a few qualitative statements regarding geometry. First, it is apparent that the slow light curve decay is not compatible with a compact region lying at low latitudes. A compact region lying near the equator would occult quickly, producing a rapid light curve decay resembling a step function (not observed). As an alternative, one might propose an extended region covering a significant fraction of the coronal area at low latitudes. But, such an extended geometry would imply a large filling factor, whereas the rather deep occultation in the light curve (peak-to-trough ratio ≈ 14) indicates that the filling factor cannot be large. Specifically, for the single loop of constant cross section discussed above ($H = 0.58R_*$, $\Gamma = 1$, $\alpha = 1$), the area filling factor is $f = A_{loop}/A_* \approx 0.03$. We thus favor a geometry in which the region responsible for the modulation lies at high latitudes, perhaps near one of the poles. Such a configuration permits the active region to span a broad range in longitude (giving the desired slow occultation) without requiring a large filling factor. Apart from these considerations, a high-latitude configuration would be expected if the coronal active region overlies photospheric spots since Doppler imaging and photometric studies indicate that polar spots are prevalent in weak-lined T Tauri stars (cf. Herbst et al. 1994).

In the above discussion, we have argued for a high-latitude active region but have at the same time shown that a *single, nonexpanding* loop must lie at a latitude below $\approx 40°$ to be *completely* occulted. These conclusions, which may appear somewhat contradictory, can be reconciled by any of the following: (1) the actual density in the flaring region may be somewhat higher than the lower limit of $n_e = 2 \times 10^{11}$ cm^{-3} used in our calculations, (2) the flaring region may consist of multiple and/or expanding loops (as Fig. 16 shows, complete occultation at a latitude of 60° could be achieved with as few as 10 expanding loops), and (3) the occultation may be partial, rather than complete. Of these possibilities, the expanding loop geometry would seem most likely since the observed DEM (Fig. 9) is heavily weighted toward the hottest plasma, which is located at the loop top in stable loop configurations. Partial occultation would seem least likely since an extrapolation of the sinusoidal light curve fit during the flare to its minimum value gives a count rate that is in good agreement with that actually observed during quiescence.

5.4. *Summary of X-Ray Variability of V773 Tau*

Two separate *ASCA* observations of V773 Tau have shown that it is highly variable in X-rays. During an intense flare on 1995 September 16–17 the peak X-ray luminosity was $L_X = 10^{32.4}$ ergs s^{-1}, which exceeds that of the quiet Sun by 5 orders of magnitude and makes this one of the strongest flares ever detected in a T Tauri star. In stark contrast, a follow-up observation taken five months later showed a state of low activity with $L_X = 10^{31.1}$ ergs s^{-1} and no large-amplitude variability. A comparison with earlier *ROSAT* observations suggests that this latter value represents a quiescent state during which L_X is at or near its minimum.

The light curve during the flare on Sep 16–17 shows a slow convex-shaped decline during which the count rate decreased by a factor of ~ 3 over a time interval of ~ 1 day. The simplest model that can reproduce the full *ASCA* light curve during the decay is a constant + sinusoid with an inferred X-ray period of 71.2 hr (= 2.97 days), which is consistent with the stellar rotation period(s) derived from optical data. At least one short-term ($\sim$ hr) increase in the hardness ratio was detected during the decay. Time-resolved spectra show that this hardness increase was accompanied by a temperature increase, providing convincing evidence that the plasma was being reheated.

The slow decline in count rate during the flare decay was mimicked by a steady drop in the emission measure of the hottest plasma component, although the temperature of this component decreased only moderately from the peak value of ≈ 42 MK measured at the start of the observation. No significant variability in the temperature or emission measure of the cool component at ≈ 10 MK was seen during the flare. This decoupling between the variability of the hot and cool components suggests that they are physically distinct.

[3] Eq. (5) follows from the more general relation below, which gives the visible loop height above the limb (H_{vis}) as a function of latitude θ and azimuthal phase angle ϕ,

$$H_{vis} = R_*[(1 + H/R_*)\sqrt{\cos^2 \theta \cos^2 \phi + \sin^2 \theta} - 1] .$$

The above equation adopts the phase convention that $\phi = 0°$ as the loop begins to move behind the limb and $\phi = 90°$ directly behind the star. The above relation is valid only for $i = 90°$ and is obviously restricted to that range of ϕ for which $H_{vis} \geq 0$.

Information derived from the *ASCA* light curves and time-resolved spectra provide a direct test of flare decay models. We have compared flare models based on the solar analogy with the observed decay profile and have also considered the relevance of unconventional models. The simplest implementation of a quasi-static cooling loop model is able to recover the observed decay of kT_2 and EM_2. However, this model cannot reproduce the convex-shaped light curve and a two-ribbon flare model encounters similar difficulties. There is no compelling need to invoke star-disk reconnection as the flare mechanism since recent theoretical models do not require wind up of the field lines and arguments in favor of a massive disk around V773 Tau are now in question. An interbinary flare seems unlikely given the wide binary separation ($a \approx 73\ R_\odot$). If the sinusoidal light curve shape is due to rotational occultation of the flaring region then a lower limit on the electron density $n_e \geq 2 \times 10^{11}\ \mathrm{cm}^{-3}$ is inferred. At this density, reheating is needed to sustain the hotter plasma at a temperature near ~ 37 MK for the duration of the observation (~ 1 day).

6. CONCLUSIONS AND OUTLOOK

We have presented *ASCA* observations of the Barnard 209 dark cloud that provide the first detection of X-ray variability in the active WTTS binary V773 Tau and in the double infrared source IRAS 04113+2758. Our analysis also yields new information on the differential emission measure distribution during a T Tauri star flare as well as valuable data on how the physical state of the flaring plasma evolves with time. These data place stringent tests on flare models.

The main conclusions of this study are the following:

1. The temperature structure of V773 Tau is bimodal with a cool component at $T_1 \approx 7$–10 MK (0.7–0.9 keV) and a hot component whose temperature varies around an average value of $T_2 \approx 37$ MK (3.2 keV). There is little if any plasma at intermediate temperatures of ~ 1–2 keV. The *ASCA* data do not rule out softer emission below ~ 0.4 keV.

2. The time-averaged temperature structure of V773 Tau is similar during quiescent and flaring states, but the hot component comprises a larger fraction of the total emission measure during flares. The presence of a hot component at flarelike temperatures even during quiescence points toward persistent low-level flaring.

3. Variability during the V773 Tau flare is restricted to the hot component, suggesting that the hot and cool components are physically distinct.

4. Metal abundances during the flare are depleted relative to solar photospheric values, with an inferred iron abundance for V773 Tau of Fe ≈ 0.2–0.3 solar. These values are similar to those derived from more extensive analyses of other active late-type stars, but the origin of this apparent metal deficiency is not yet understood.

5. Flare models based on the solar analogy (quasi-static cooling loops and two-ribbon flares) are unable to reproduce the convex-shaped *ASCA* light curve. Difficulties have also been encountered in applying these models to slowly decaying flares in RS CVn binaries (Graffagnino et al. 1995; Kürster & Schmitt 1996). It is thus not yet clear if these slow flares have a solar analog, and our analysis indicates that some or all of the following complexities may be present: (1) reheating of the hot plasma during the decay phase via low-level secondary events, (2) nontrivial flare geometries (e.g., multiple and/or expanding loops), and (3) dynamical effects (e.g., rotational modulation) that may be superimposed on the intrinsic flare decay profile.

6. There are no compelling arguments in favor of either a star-disk flare or an interbinary flare interpretation for the V773 outburst. However, given the close similarity between the V773 Tau flare and the slow flares that have been detected in close RS CVn binaries (Graffagnino et al. 1995; Kürster & Schmitt 1996), further investigation of the interbinary hypothesis is warranted. In particular, numerical models that investigate the evolution of loops extending into the interbinary region where the perturbative effect of the companion star becomes important are needed. Also, X-ray observations of close T Tauri binaries in eccentric orbits with good orbital phase coverage are needed in order to determine if increased X-ray activity occurs near periastron. Recurrent optical brightening near periastron has recently been reported for the classical T Tauri binary system DQ Tau (Mathieu et al. 1997), and may signal interaction between its two components.

The variability that was detected in V773 Tau during our initial observation in 1995 September was most likely due to the slow decay of an intense flare in which the volume containing the flaring plasma was being progressively occulted by stellar rotation. The sinusoidal shape of the *ASCA* light curve during the flare decay provides the most compelling evidence to date for rotational X-ray modulation in a weak-lined T Tauri star, but this evidence cannot be taken as conclusive since our observation spans only one-third of a rotation cycle. Further X-ray observations of the most active WTTS over many rotation cycles are needed to search for unambiguous evidence of X-ray modulation. It is noteworthy that rotational X-ray modulation has recently been reported in young late-type stars such as EK Draconis (Güdel et al. 1995) and AB Doradus (Kürster et al. 1997). In the case of WTTS, high priority should be given to long-term X-ray monitoring of those stars with rotationally modulated optical light curves such as V773 Tau and V410 Tau (Strom & Strom 1994). The confirmation of rotational X-ray modulation in such objects would open up a new line of research into the atmospheric structure of T Tauri stars. In particular, the geometrical relationship between surface spots and coronal active regions could be explored through simultaneous optical and X-ray observations, as is now being done for RS CVn systems (cf. Hempelmann et al. 1997).

This work was supported by NASA grant NAG 5-3224. We acknowledge useful discussions with S. Drake, M. Gagné, J.-F. Lestrade, R. Kopp, and A. Welty. We also thank J. Linsky for a critical reading of the manuscript as well as members of the *ASCA* operations, instrument calibration and software support teams, who have made this study possible. This research has made use of the Statistical Consulting Center for Astronomy at Penn State as well as the SIMBAD astronomical database operated by CDS at Strasbourg, France.

REFERENCES

Anders, E., & Grevesse, N. 1989, Geochim. Cosmochim. Acta, 53, 197
Basri, G., Marcy, G. W., & Valenti, J. A. 1992, ApJ, 390, 662
Beckwith, S. V. W., Sargent, A. I., Chini, R., & Güsten, R. 1990, AJ, 99, 924
Bertout, C. 1989, ARA&A, 27, 351
Brickhouse, N., et al. 1995, Legacy, 6, 4
Brown, A., Skinner, S. L., Stewart, R. T., & Jones, K. L. 1996, in Magnetodynamic Phenomena in the Solar Atmosphere—Prototypes of Stellar Magnetic Activity, ed. Y. Uchida, T. Kosugi, & H. S. Hudson (Dordrecht: Kluwer), 279
Cabrit, S., Edwards, S., Strom, S. E., & Strom, K. M. 1990, ApJ, 354, 687
Dotani, T., Mitsuda, K., Ezuka, H., Hayashida, K., Torii, K., Miura, N., Otani, C., Crew, G., Rasmussen, A., & Gendreau, K. 1996, ASCANEWS (Greenbelt: NASA GSFC), 4, 3
Dutrey, A., Guilloteau, S., Duvert, G., Prato, L., Simon, M., Schuster, K., & Ménard, F. 1996, A&A, 309, 493
Duvert, G., Cernicharo, J., & Baudry, A. 1986, A&A, 164, 349
Feigelson, E. D., Welty, A. D., Imhoff, C. L., Hall, J. C., Etzel, P. B., Phillips, R. B., & Lonsdale, C. J. 1994, ApJ, 432, 373
Gagné, M., Caillault, J.-P., & Stauffer, J. R. 1995, ApJ, 445, 280
Ghez, A. M., Neugebauer, G., & Matthews, K. 1993, AJ, 106, 2005
Ghosh, P., & Lamb, F. K. 1979, ApJ, 232, 259
Golub, L., Maxson, C., Rosner, R., Serio, S., & Vaiana, G. S. 1980, ApJ, 238, 343
Gorenstein, P. 1975, ApJ, 198, 95
Gotthelf, E. 1996, ASCANEWS (Greenbelt: NASA GSFC), 4, 31
Graffagnino, V. G., Wonnacott, D., & Schaeidt, S. 1995, MNRAS, 276, 263
Güdel, M., Benz, A. O., Schmitt, J. H. M. M., & Skinner, S. L. 1996, ApJ, 471, 1002
Güdel, M., Guinan, E. F., Mewe, R., Kaastra, J., & Skinner, S. L. 1997, ApJ, 479, 416
Güdel, M., & Schmitt, J. H. M. M. 1996, in MPE Rep. 263, Röntgenstrahlung from the Universe, ed. H. Zimmermann, J. Trümper, & H. Yorke (Garching: MPE), 35
Güdel, M., Schmitt, J. H. M. M., Benz, A. O., & Elias, N. M. 1995, A&A, 301, 201
Hartigan, P., Strom, K. M., & Strom, S. E. 1994, ApJ, 427, 961
Hempelmann, A., Hatzes, A. P., Kürster, M., & Patkós, L. 1997, A&A, 317, 125
Herbig, G. H., & Bell, K. R. 1988, Lick Obs. Bull. 1111, Third Catalog of Emission-Line Stars of the Orion Population (Santa Cruz: Univ. California)
Herbst, W., Herbst, D. K., Grossman, E. J., & Weinstein, D. 1994, AJ, 108, 1906
Jensen, E. L., Mathieu, R. D., & Fuller, G. A. 1996, ApJ, 458, 312
Kaastra, J. S., Mewe, R., Liedahl, D. A., Singh, K. P., White, N. E., & Drake, S. A. 1996a, A&A, 314, 547
Kaastra, J. S., Mewe, R., & Nieuwenhuijzen, H. 1996b, in UV and X-ray Spectroscopy of Astrophysical and Laboratory Plasmas, ed. K. Yamashita & T. Watanabe (Univ. Acad. Press), 411
Kenyon, S. J., Hartmann, L. W., Strom, K. M., & Strom, S. E. 1990, AJ, 99, 869
Kopp, R. A., & Poletto, G. 1984, Sol. Phys., 93, 351
Kürster, M., & Schmitt, J. H. M. M. 1996, A&A, 311, 211
Kürster, M., Schmitt, J. H. M. M., Cutispoto, G., & Dennerl, K. 1997, A&A, 320, 381
Lang, K. R. 1980, Astrophysical Formulae (New York: Springer), 286
Leinert, Ch., Zinnecker, H., Weitzel, N., Christou, J., Ridgway, S. T., Jameson, R., Haas, M., & Lenzen, R. 1993, A&A, 278, 129
Lestrade, J.-F., Jones, D. L., Phillips, R. B., Titus, M. A., Preston, R. A., Rioja, M., & Gabuzda, D. C. 1997, in preparation
Lynds, B. T. 1962, ApJS, 7, 1
Maggio, A., & Peres, G. 1996, A&A, 306, 563
Martín, E. L., Rebolo, R., Magazzu, A., & Pavlenko, Ya.V. 1994, A&A, 282, 503
Mathieu, R. D., Stassun, K. Basri, G., Jensen, E. L. N., Johns-Krull, C. M., Valenti, J. A., & Hartmann, L. W. 1997, AJ, 113, 1841
Mewe, R. 1996, Sol. Phys., 169, 335
Mewe, R., Kaastra, J. S., & Liedahl, D. A. 1995, Legacy, 6, 16
Mewe, R., Kaastra, J. S., van den Oord, G. H. J., Vink, J., & Tawara, Y. 1997, A&A, 320, 147
Moriarty-Schieven, G. H., Wannier, P. G., Tamura, M., & Keene, J. 1992, ApJ, 400, 260
Morrison, R., & McCammon, D. 1983, ApJ, 270, 119
Neuhäuser, R., Sterzik, M. F., Schmitt, J. H. M. M., Wichmann, R., & Krautter, J. 1995, A&A, 297, 391
Osterloh, M., & Beckwith, S. V. W. 1995, ApJ, 439, 288
Ottmann, R., Schmitt, J. H. M. M., & Kürster, M. 1993, ApJ, 413, 710
Phillips, R. B., Lonsdale, C. J., Feigelson, E. D., & Deeney, B. D. 1996, AJ, 111, 918
Poletto, G., Pallavicini, R., & Kopp, R. A. 1988, A&A, 201, 93
Preibisch, T., Neuhäuser, R., & Alcalá, J. M. 1995, A&A, 304, L13
Prusti, T., Clark, F. O., Laureijs, R. J., Wakker, B. P., & Wesselius, P. R. 1992, A&A, 259, 537
Rydgren, A. E., & Vrba, F. J. 1983, ApJ, 267, 191
Schmitt, J. H. M. M. 1996, in IAU Symp. 176, Stellar Surface Structure, ed. K. G. Strassmeier & J. L. Linsky (Dordrecht: Kluwer), 85
Schrijver, C. J., Mewe, R., van den Oord, G. H. J., & Kaastra, J. S. 1995, A&A, 302, 438
Serio, S., Peres, G., Vaiana, G. S., Golub, L., & Rosner, R. 1981, ApJ, 243, 288
Shu, F., Najita, J., Ostriker, E., Wilkin, F., Ruden, S., & Lizano, S. 1994, ApJ, 429, 781
Simon, T., Linsky, J. L., & Schiffer, F. H. 1980, ApJ, 239, 911
Skinner, S. L., Brown, A., & Walter, F. M. 1991, AJ, 102, 1742
Smith, K. W., Bonnell, I. A., & Lewis, G. F. 1995, MNRAS, 276, 263
Strom, K. M., & Strom, S. E. 1994, ApJ, 424, 237
Strom, K. M., Strom, S. E., Edwards, S., Cabrit, S., & Skrutskie, M. F. 1989, AJ, 97, 1451
Tamura, M., Gatley, I., Waller, W., & Werner, M. W. 1991, ApJ, 374, L25
Tanaka, Y., Inoue, H., & Holt, S. S. 1994, PASJ, 46, L37
van den Oord, G. H. J. 1988, A&A, 205, 167
van den Oord, G. H. J., & Mewe, R. 1989, A&A, 213, 245 (vdOM89)
———. 1997, A&A, submitted
van den Oord, G. H. J., Mewe, R., & Brinkman, A. C. 1988, A&A, 205, 181
Welty, A. D. 1995, AJ, 110, 776
White, N. E. 1996, in Proc. Ninth Camb. Workshop on Cool Stars, Stellar Systems and the Sun, R. Pallavicini & A. Dupree, San Francisco: ASP, 193
White, N. E., et al. 1994, PASJ, 46, L97
White, S. M., Pallavicini, R., & Kundu, M. R. 1992, A&A, 259, 149
Wolk, S. J., & Walter, F. M. 1996, AJ, 111, 2066